a clone[29]; the HTLV-1 genomic integration site may contribute a similar advantage.[26]

A further unexpected observation was the preferential survival in vivo of the HTLV-1 provirus in the acrocentric chromosomes 13, 14, 15, 21, and (although not reaching formal significance) 22. Throughout most of the cell cycle, these chromosomes are physically associated with the nucleolus, and they encode the machinery of the ribosome on the short (p) arm. Because the HTLV-1 proviral integration sites are found only in the long (q) arm of these chromosomes, we postulate that the selective advantage enjoyed by these clones derives not from the proviral integration near the ribosome-coding genes but rather from the physical location of the provirus-containing chromatin in the nucleus, perhaps by coupling proviral transcription to transcription of the acrocentric chromosomes. Experiments are underway to test this hypothesis.

Acknowledgments

The authors thank Nirav Malani and Frederic D. Bushman at the department of Microbiology, University of Pennsylvania, Philadelphia, PA for the list of random integration sites and for developing software packages and the Core Genomics Laboratory at the MRC Clinical Sciences Centre, Hammersmith Hospital, London, United Kingdom. The authors thank Aileen Rowan and Yorifumi Satou for many helpful discussion and comments and the patient donors in Japan.

This work was funded by Leukaemia and Lymphoma Research and the Wellcome Trust.

Authorship

Contribution: L.B.C., G.P.T., M.M., and C.R.M.B. conceived and designed the experiments; M.M. performed the clinical diagnosis; L.B.C. performed the experiments; M.V. and L.F. performed and interpreted TCR studies; L.B.C. analyzed the data; A.M., H.N., and D.J.L. contributed to the bioinformatic and statistical analysis, tools, and data sets; and L.B.C. and C.R.M.B. wrote the paper.

Conflict-of-interest disclosure: The authors declare no competing financial interests.

Correspondence: Charles R. M. Bangham, Wright-Fleming Institute, Imperial College, Norfolk Place, London, W2 1PG, United Kingdom; e-mail: c.bangham@imperial.ac.uk.

References

1. Shimoyama M. Diagnostic criteria and classification of clinical subtypes of adult T-cell leukaemia-lymphoma. A report from the Lymphoma Study Group (1984-87). *Br J Haematol.* 1991;79(3):428-437.
2. Sasaki D, Doi Y, Hasegawa H, et al. High human T cell leukemia virus type-1(HTLV-1) provirus load in patients with HTLV-1 carriers complicated with HTLV-1-unrelated disorders. *Virol J.* 2010;7:81.
3. Iwanaga M, Watanabe T, Utsunomiya A, et al; Joint Study on Predisposing Factors of ATL Development investigators. Human T-cell leukemia virus type I (HTLV-1) proviral load and disease progression in asymptomatic HTLV-1 carriers: a nationwide prospective study in Japan. *Blood.* 2010;116(8):1211-1219.
4. Demontis MA, Hilburn S, Taylor GP. Human T cell lymphotropic virus type 1 viral load variability and long-term trends in asymptomatic carriers and in patients with human T cell lymphotropic virus type 1-related diseases. *AIDS Res Hum Retroviruses.* 2013;29(2):359-364.
5. Overbaugh J, Bangham CR. Selection forces and constraints on retroviral sequence variation. *Science.* 2001;292(5519):1106-1109.
6. Gillet NA, Malani N, Melamed A, et al. The host genomic environment of the provirus determines the abundance of HTLV-1-infected T-cell clones. *Blood.* 2011;117(11):3113-3122.
7. Cook LB, Rowan AG, Melamed A, Taylor GP, Bangham CR. HTLV-1-infected T cells contain a single integrated provirus in natural infection. *Blood.* 2012;120(17):3488-3490.
8. Tsukasaki K, Tsushima H, Yamamura M, et al. Integration patterns of HTLV-I provirus in relation to the clinical course of ATL: frequent clonal change at crisis from indolent disease. *Blood.* 1997;89(3):948-956.
9. Matsuoka M, Jeang KT. Human T-cell leukemia virus type 1 (HTLV-1) and leukemic transformation: viral infectivity, Tax, HBZ and therapy. *Oncogene.* 2011;30(12):1379-1389.
10. Bangham CR. CTL quality and the control of human retroviral infections. *Eur J Immunol.* 2009; 39(7):1700-1712.
11. Nagai M, Usuku K, Matsumoto W, et al. Analysis of HTLV-I proviral load in 202 HAM/TSP patients and 243 asymptomatic HTLV-I carriers: high proviral load strongly predisposes to HAM/TSP. *J Neurovirol.* 1998;4(6):586-593.
12. Jeffery KJ, Usuku K, Hall SE, et al. HLA alleles determine human T-lymphotropic virus-I (HTLV-I) proviral load and the risk of HTLV-I-associated myelopathy. *Proc Natl Acad Sci USA.* 1999;96(7): 3848-3853.
13. Melamed A, Laydon DJ, Gillet NA, Tanaka Y, Taylor GP, Bangham CR. Genome-wide determinants of proviral targeting, clonal abundance and expression in natural HTLV-1 infection. *PLoS Pathog.* 2013;9(3):e1003271.
14. Nosaka K, Maeda M, Tamiya S, Sakai T, Mitsuya H, Matsuoka M. Increasing methylation of the CDKN2A gene is associated with the progression of adult T-cell leukemia. *Cancer Res.* 2000;60(4): 1043-1048.
15. Kwok S, Ehrlich G, Poiesz B, Kalish R, Sninsky JJ. Enzymatic amplification of HTLV-I viral sequences from peripheral blood mononuclear cells and infected tissues. *Blood.* 1988;72(4): 1117-1123.
16. Tamiya S, Matsuoka M, Etoh K, et al. Two types of defective human T-lymphotropic virus type I provirus in adult T-cell leukemia. *Blood.* 1996; 88(8):3065-3073.
17. Takeda S, Maeda M, Morikawa S, et al. Genetic and epigenetic inactivation of tax gene in adult T-cell leukemia cells. *Int J Cancer.* 2004;109(4): 559-567.
18. Barski A, Cuddapah S, Cui K, et al. High-resolution profiling of histone methylations in the human genome. *Cell.* 2007;129(4):823-837.
19. Sadelain M, Papapetrou EP, Bushman FD. Safe harbours for the integration of new DNA in the human genome. *Nat Rev Cancer.* 2012;12(1): 51-58.
20. Laydon DJ, Melamed A, Sim A, et al. Quantification of HTLV-1 clonality and TCR diversity. *PLOS Comput Biol.* In press.
21. Gini C. Variabilita e Mutuabilita. Contributo allo Studio delle Distribuzioni e delle Relazioni Statistiche. Bologna, Italy: C. Cuppini; 1912.
22. Handcock M, Morris M. Relative Distribution Methods in the Social Sciences. New York, NY: Springer-Verlag; 1999.
23. Presson AP, Kim N, Xiaofei Y, Chen IS, Kim S. Methodology and software to detect viral integration site hot-spots. *BMC Bioinformatics.* 2011;12:367.
24. Berry CC, Gillet NA, Melamed A, Gormley N, Bangham CR, Bushman FD. Estimating abundances of retroviral insertion sites from DNA fragment length data. *Bioinformatics.* 2012;28(6): 755-762.
25. Meekings KN, Leipzig J, Bushman FD, Taylor GP, Bangham CR. HTLV-1 integration into transcriptionally active genomic regions is associated with proviral expression and with HAM/TSP. *PLoS Pathog.* 2008;4(3):e1000027.
26. Bangham CRM, Cook LB, Melamed A. HTLV-1 clonality in adult T-cell leukaemia and non-malignant HTLV-1 infection [published online ahead of print December 6, 2013]. *Semin Cancer Biol.*
27. Melamed A, Witkover AD, Laydon DJ, et al. Clonality of HTLV-2 in natural infection. *PLoS Pathog.* 2014;10(3):e1004006.
28. Macnamara A, Rowan A, Hilburn S, et al. HLA class I binding of HBZ determines outcome in HTLV-1 infection. *PLoS Pathog.* 2010;6(9): e1001117.
29. Vogelstein B, Papadopoulos N, Velculescu VE, Zhou S, Diaz LA Jr, Kinzler KW. Cancer genome landscapes. *Science.* 2013;339(6127): 1546-1558.

blood 2014 123: 3925-3931
doi:10.1182/blood-2014-02-553602 originally published online April 15, 2014

The role of HTLV-1 clonality, proviral structure, and genomic integration site in adult T-cell leukemia/lymphoma

Lucy B. Cook, Anat Melamed, Heather Niederer, Mikel Valganon, Daniel Laydon, Letizia Foroni, Graham P. Taylor, Masao Matsuoka and Charles R. M. Bangham

Blood (print ISSN 0006-4971, online ISSN 1528-0020), is published weekly by the American Society of Hematology, 2021 L St, NW, Suite 900, Washington DC 20036.

Published OnlineFirst October 31, 2013; DOI: 10.1158/0008-5472.CAN-13-0436

Molecular and Cellular Pathobiology

Cancer Research

HTLV-1 bZIP Factor Suppresses Apoptosis by Attenuating the Function of FoxO3a and Altering Its Localization

Azusa Tanaka-Nakanishi, Jun-ichirou Yasunaga, Ken Takai, and Masao Matsuoka

Abstract

As the infectious agent causing human adult T-cell leukemia (ATL), the human T-cell leukemia virus type 1 (HTLV-1) virus spreads *in vivo* primarily by cell-to-cell transmission. However, the factors that determine its transmission efficiency are not fully understood. The viral genome encodes the HTLV-1 bZIP factor (HBZ), which is expressed in all ATL cases and is known to promote T-cell proliferation. In this study, we investigated the hypothesis that HBZ also influences the survival of T cells. Through analyzing the transcriptional profile of HBZ-expressing cells, we learned that HBZ suppressed transcription of the proapoptotic gene *Bim* (*Bcl2l11*) and that HBZ-expressing cells were resistant to activation-induced apoptosis. Mechanistic investigations into how HBZ suppresses *Bim* expression revealed that HBZ perturbs the localization and function of FoxO3a, a critical transcriptional activator of the genes encoding Bim and also Fas ligand (FasL). By interacting with FoxO3a, HBZ not only attenuated DNA binding by FoxO3a but also sequestered the inactive form of FoxO3a in the nucleus. In a similar manner, HBZ also inhibited *FasL* transcription induced by T-cell activation. Further study of ATL cells identified other Bim perturbations by HBZ, including at the level of epigenetic alteration, histone modification in the promoter region of the Bim gene. Collectively, our results indicated that HBZ impairs transcription of the *Bim* and *FasL* genes by disrupting FoxO3a function, broadening understanding of how HBZ acts to promote proliferation of HTLV-1–infected T cells by blocking their apoptosis. *Cancer Res; 74(1); 188–200. ©2013 AACR.*

Introduction

Human T-cell leukemia virus type 1 (HTLV-1) is estimated to infect 10 to 20 million people in the world (1). This virus causes not only a neoplastic disease of $CD4^+$ T cells, adult T-cell leukemia (ATL), but also chronic inflammatory diseases of the central nervous system, lung, or skin (2). HTLV-1 can be transmitted efficiently in a cell-to-cell fashion (3, 4), whereas free virus shows poor infectivity (5, 6), and virions are not detected in infected individuals. To increase the number of infected cells and facilitate transmission, HTLV-1 increases its copy number primarily by triggering the proliferation of infected cells, replicating within the host genome instead of undergoing viral replication (7, 8). Thus, HTLV-1 promotes proliferation and suppresses apoptosis of infected cells via complex interactions of viral proteins with host factors.

Among the viral genes encoded in HTLV-1, the *tax* gene has been extensively studied. Tax can activate various signal pathways like NF-κB, AP-1, and SRF (9). However, Tax expression is frequently undetectable in ATL cases. Importantly, the nonsense mutations in the *tax* gene are often observed in not only ATL cases but also infected cells of asymptomatic HTLV-1 carriers (10). These findings suggest that other mechanisms suppress the apoptosis of HTLV-1–infected cells in the absence of Tax expression (2). We have reported that the *HTLV-1 bZIP factor (HBZ)* gene is expressed in all ATL cases (11). Furthermore, HBZ promotes the proliferation of T cells and induces development of T-cell lymphomas and inflammatory diseases in transgenic mice (12). Therefore, we speculated that HBZ might also influence apoptosis.

There are two major pathways for apoptosis: the extrinsic and intrinsic apoptotic pathways, which are mediated by Fas and Bim, respectively (13). ATL cells are known to express high levels of Fas antigen, and are susceptible to Fas-mediated signaling (14). However, FasL expression is suppressed in ATL cells by silencing of the *early growth response 3* (*EGR3*) gene transcription, a phenomenon that enables ATL cells to escape activation-induced cell death (15). In addition, Tax increases expression of c-FLIP, which confers resistance to Fas-mediated apoptosis (16, 17). Furthermore, activation of NF-κB by Tax also enables HTLV-1–infected cells to be resistant to apoptosis (18). To date, the effects of HTLV-1 infection on Bim-mediated apoptosis remain unknown.

In this study, we analyzed transcriptional changes induced by HBZ expression in T cells, and found that transcription of a proapoptotic gene, *Bim*, was hindered by HBZ. This suppression led to decreased activation-induced cell death. We found that HBZ suppressed *Bim* transcription by targeting FoxO3a, a critical transcription factor for the *Bim* and *FasL* gene. In some

Authors' Affiliation: Laboratory of Virus Control, Institute for Virus Research, Kyoto University, Sakyo-ku, Kyoto, Japan

Note: Supplementary data for this article are available at Cancer Research Online (http://cancerres.aacrjournals.org/).

Corresponding Author: M. Matsuoka, Institute for Virus Research, Kyoto University, 53 Shogoin Kawahara-cho, Sakyo-ku, Kyoto 606-8507, Japan. Phone: 81-757-514-048; Fax: 81-757-514-049; E-mail: mmatsuok@virus.kyoto-u.ac.jp

doi: 10.1158/0008-5472.CAN-13-0436

Published OnlineFirst October 31, 2013; DOI: 10.1158/0008-5472.CAN-13-0436

ATL cell lines and ATL cases, the *Bim* gene transcription was also silenced by epigenetic mechanisms, but this phenomenon seemed to be secondary to HBZ-mediated suppression of transcription. Thus, it is suggested that HBZ suppresses both intrinsic and extrinsic apoptotic pathways and contributes to the proliferation of ATL cells.

Materials and Methods

Cell lines and clinical samples

HTLV-1 immortalized cell lines (MT-4), ATL cell lines (ED, TL-Oml, and MT-1), T-cell lines not infected with HTLV-1 (Jurkat, SupT1, and CCRF-CEM) were cultured in RPMI 1640 medium supplemented with 10% FBS and antibiotics at 37°C under a 5% CO_2 atmosphere. Jurkat cells stably expressing spliced form of HBZ (sHBZ), Jurkat-HBZ, were maintained as described previously (19). To construct CCRF-CEM cells stably expressing HBZ, CEM-HBZ, the coding sequence of HBZ was subcloned into pME18Sneo vector and then the expression vector or its empty vector were transfected into CCRF-CEM cells by using Neon (Invitrogen) according to the manufacturer's instructions. Stable transfectants were selected in G418 (1 mg/mL). 293T cells were cultured in Dulbecco's Modified Eagle Medium supplemented with 10% FBS and antibiotics and when 293FT cells were cultured, 500 μg/mL G418 was added. Fas-blocking antibody was purchased from Alexis.

This study was conducted according to the principles expressed in the Declaration of Helsinki. The study was approved by the Institutional Review Board of Kyoto University (G204). All patients provided written informed consent for the collection of samples and subsequent analysis.

Plasmid constructs

Wild-type form of FoxO3a was generated by PCR amplification using Jurkat cDNA library and constitutively active form of FoxO3a (FoxO3aAAA) was also generated by PCR amplification with mutated primers (20). These PCR fragments were then subcloned into pCMV-Tag2B vector and pIRES-hrGFP-1a (Stratagene). The vectors encoding the myc-His-tagged form of HBZ and its mutants used in this study have been described previously (19, 21). We modified pLKO.1-EGFP vector for delivery of anti-FoxO3 short hairpin RNAs (shRNA) to Jurkat, Jurkat-control, and Jurkat-HBZ. shRNA sequence used was 5′-GCACAACCTGTCCTGCATAG-3′. The 6xDBE-Luc construct that contains six FOXO-binding sites known as DAF-16 binding elements (DBE) was kindly provided by Dr. Furuyama (Kagawa Prefectural University of Health Sciences, Kagawa, Japan) and the backbone of this vector was pGL3-basic (Promega; ref. 22).

Luciferase assay

Jurkat cells were transfected with 0.2 μg/well of luciferase reporter plasmid, 1 ng/well of *Renilla* luciferase control vector (phRL-TK), 0.2 μg/well of FoxO3aAAA expression plasmid or its empty vector, and 0.6 μg/well of HBZ expression plasmid or its empty vector with caspase inhibitor Z-VAD-FMK (MBL). Plasmids were transfected using Neon (Invitrogen) according to the manufacturer's instructions. After 24 hours, cells were collected and luciferase activities were measured using the Dual-Luciferase Reporter Assay (Promega). Relative luciferase activity was calculated as the ratio of firefly to *Renilla* luciferase activity. Three independent experiments, each with triplicate transfections, were performed and typical results are shown.

Microarray analysis

Jurkat-control and Jurkat-HBZ were stimulated with phorbol myristate acetate (PMA; 50 ng/mL) and ionomycin (Io; 1 μg/mL) for 9 hours. After the stimulation, cells were collected and total RNA was isolated using TRIzol Reagent (Invitrogen) according to the manufacturer's instructions. We then digested DNA using deoxyribonuclease I (Invitrogen) and cleaned up RNA using RNeasy Mini Kit (Qiagen) according to the manufacturer's instructions. We then synthesized cDNA and performed microarray processing according to the GeneChip Expression Analysis Technical Manual (Affymetrix). All data were analyzed by using GeneSpring GX (Agilent Technologies). The microarray data related to this article have been submitted to the Gene Expression Omnibus under the accession number GSE48029.

Immunofluorescence analysis

293FT cells were transfected with expression vectors using Lipofectamine LTX (Invitrogen) or TransIT (TaKaRa). Twenty-four hours after transfection, cells were reseeded on the poly-L-lysine–coated glass (Matsunami Glass Ind., Ltd.) or poly-D-lysine (Sigma)–coated glass. Twenty-four hours after the reseeding, cells were fixed with 4% paraformaldehyde for 15 minutes and permeabilized with 0.2% Triton X-100 for 15 minutes, and blocked by incubation in 5% BSA/PBS for 30 minutes. For immunostaining, the cells were incubated with anti-Foxo3a, anti-p-Foxo3a (Cell Signaling Technology), Cy3-conjugated anti-c-Myc (Sigma) or biotinylated anti-FLAG (Sigma) antibodies for 1 hour or in case of observation of endogenous expression, cells were incubated overnight at 4°C. Primary antibodies were visualized by incubating the cells with Alexa-Fluor 488–conjugated goat anti-rabbit immunoglobulin G (IgG) antibody (Invitrogen) or AlexaFluor 488–conjugated streptavidin (Invitrogen). Nuclei were stained and mounted with ProLong Gold antifade reagent with 4′,6-diamidino-2-phenylindole (DAPI; Invitrogen). To concentrate nonadherent cells onto a microscope slide, CytoFuge (StatSpin) was used. Fixation and blocking were performed as described earlier.

Assessment of apoptosis

Apoptotic cells were routinely identified by Annexin V-APC (eBioscience) or phycoerythrin (PE) or fluorescein isothiocyanate (FITC; BioVision) -staining according to the manufacturer's instructions and analyzed with a flow cytometer (BD FACSCanto II; BD Biosciences). Data files were analyzed by using FlowJo software (TreeStar).

Real-time PCR

Total RNA was isolated for the analysis using TRIzol reagent. RNA was treated with DNase I to eliminate the genomic DNA. Reverse transcription was performed using random primer and SuperScript III Reverse Transcriptase (Invitrogen). $CD25^-$ $CD4^+$ cells from healthy donor were obtained by using human

Published OnlineFirst October 31, 2013; DOI: 10.1158/0008-5472.CAN-13-0436

CD4 T Lymphocyte Enrichment kit (BD Pharmingen). Then, cells were stimulated with PMA/Io for 9 hours, RNA was isolated, and reverse transcription was performed as described earlier. cDNA products were analyzed by real-time PCR using the Taqman Universal PCR Master Mix (PE Applied Biosystems) or FastStart Universal SYBR Green Master (Roche) and Applied Biosystems StepOnePlus Real-Time PCR System according to the manufacturer's instructions. Specific primers and Taqman probes for the *Bim* gene, *FasL* gene, and *GAPDH* internal control gene were purchased from Applied Biosystems. Primer sequences for the *HBZ* gene and *GAPDH* gene used for the evaluation of the knockdown efficiency in MT-1 cells have been described previously (11, 23). Primer sequences for the *HBZ* gene used for another experiment to evaluate the HBZ expression in Jurkat-HBZ, MT-1, TL-Om1, and ED cells were 5′-ATGGCGGCCTCAGGGCTGTT-3′ and 5′-GCGGCTTTCCTCTTCTAAGG-3′. Primer sequences for the *FoxO3a* gene used were 5′-ACAAACGGCTCACTCTGTCCCAG-3′ and 5′-AGCTCTTGCCAGTTCCCTCATTCTG-3′. All amplifications were conducted in triplicates. The relative quantification was calculated according to the method described in Applied Biosystems ABI prism 7700 SDS User Bulletin #2.

Chromatin immunoprecipitation analysis

Chromatin immunoprecipitation (ChIP) assay was performed according to the protocol recommended by Millipore. Cells were fixed with 1% formaldehyde for 10 minutes at room temperature, washed twice with ice-cold PBS, treated with SDS-lysis buffer (1% SDS, 50 mmol/L EDTA, and 200 mmol/L Tris-HCl) for 10 minutes on ice and then sonicated. Thereafter, the DNA/protein complexes were immunoprecipitated with antibodies specific for acetylated-Histone H3, acetylated-Histone H4, dimethylated-Histone H3 (Lys4), RNA polymerase II clone CTD4H8 (Millipore), trimethylated-Histone H3 (Lys27), anti-trimethyl-Histone H3 (Lys9) antibodies (Cell Signaling Technology), or normal rabbit IgG (Santa Cruz Biotechnology) overnight at 4°C. Immune complexes were collected with salmon sperm DNA-protein A and G Sepharose slurry, washed, and eluted with freshly prepared elution buffer (1% SDS, 100 mmol/L $NaHCO_3$). Protein-DNA complexes were de-cross-linked at 65°C for 4 hours. DNA was purified and subjected to real-time PCR for quantification of the target fragments. Sequences for the primer set are described previously (24, 25). For the evaluation of binding of FoxO3a to the FOXO-binding sites, 293T cells were transfected with 5 μg of 6xDBE-Luc construct, 5 μg of FoxO3aAAA expression plasmid together with or without 5 μg of HBZ plasmid using TransIT in 10-cm dishes. Anti-FLAG (Sigma) antibody was used for the immunoprecipitation. Primers used were 5′-AGTGCAGGTGCCAGAACATT-3′ and 5′-GCCTTATGCAGTTGCTCTCC-3′, which were constructed inside of the pGL3-basic vector. For the evaluation of the DNA-binding capacity of FoxO3a with or without HBZ, expression vectors for the HA-tagged FoxO3a and Flag-tagged HBZ were transiently cotransfected into 293T cells using the TransIT reagent. Twenty-four hours after the transfection, cells were collected and chromatin immunoprecipitation assay was performed as described earlier. For the immunoprecipitation, anti-HA (Sigma) antibody was used. Primers used for *Bim* gene promoter were 5′-CCACCACTTGATTCTTGCAG-3′ and 5′-TCCAGCGCTAGTCTTCCTTC-3′, which were constructed to contain the FOXO-binding sequence located in intron1. Primers used for *FasL* gene promoter were 5′-ACGATAGCACCACTGCACTCC-3′ and 5′-GGCTGCAAACCAGTGGAAC-3′, which were also constructed to contain the three FOXO-binding sequences.

Individual PCRs were carried out in triplicate to control for PCR variation and mean C_t values were collected. Fold difference of the antibody-bound fraction (IP) versus a fixed amount of input (In) was calculated as

$$\mathrm{IP/In} = 2^{-\Delta\Delta C_t} = 2^{-(C_t(\mathrm{IP}) - C_t(\mathrm{In}))}$$

Then, the fold difference value for a target antibody (t) was subtracted by the nonspecific value derived from mouse or rabbit IgG (t_0):

$$(\mathrm{IP/In})^{t} - (\mathrm{IP/In})^{t_0}$$

Bisulfite genomic sequencing

Sodium bisulfite treatment of genomic DNA was performed as described previously (26). DNA regions were amplified using bisulfite-treated genomic DNA by nested PCR. To amplify promoter region (promoter 1) of *Bim*, primers used in the first PCR were 5′-TTTAGAGGGAGGAGAGTTTAAAG-3′ and 5′-CCCTACAACCCAACTCTAACTA-3′. Primers for the second PCR were 5′-AGGGTATAGTGAGAGCGTAGG-3′ and 5′-CAACTCTAACTAACGACCCC-3′. For promoter, two primers used in the first PCR were 5′-GTGTGATTGTTTTTTGAGGG-3′ and 5′-AAAATACCCCCAAACAAAATAC-3′. Primers for the second PCR were 5′-GCGGATTTAGTTGTAGATTTTG-3′ and 5′-ACTCTTTACCCAAAACAAACTTC-3′. PCR products were purified, cloned into pGEM-T Easy vector (Promega), and sequenced using the ABI PRISM 3130 Genetic Analyzer. For CpG methylation analysis, Web-based bisulfite sequencing analysis tool called QUMA (quantification tool for methylation analysis) was used (27).

Coimmunoprecipitation assay, analysis of the p-FoxO3a localization, and immunoblotting

Expression vectors for the relevant genes were transiently cotransfected into 293T cells using the TransIT reagent. Forty-eight hours later, cells were collected and coimmunoprecipitation assays were performed as described previously (28). For the analysis of the p-FoxO3a localization, nuclear and cytoplasmic proteins were extracted using Nuclear Complex Co-IP Kit (Active Motif). The proteins were subjected to SDS-PAGE analysis followed by immunoblotting with various antibodies. Antibodies used were anti-p-FoxO3a, anti-α-tubulin (Sigma), anti-FLAG, anti-HA (Sigma), and anti-His (Marine Biological Laboratory).

Lentiviral vector construction and transfection of the recombinant lentivirus

Lentiviral vector expressing shRNA against HBZ was constructed and recombinant lentivirus was infected as described previously (11). When more than 90% of cells expressed

Published OnlineFirst October 31, 2013; DOI: 10.1158/0008-5472.CAN-13-0436

enhanced green fluorescent protein (EGFP), the *HBZ* and *Bim* gene expressions were analyzed by real-time PCR.

Results

The *Bim* gene transcription is suppressed in HBZ-expressing Jurkat and CCRF-CEM cells

To determine the effects of HBZ on gene expression, we first performed microarray analysis. Jurkat cells with or without expression of spliced form of HBZ (Jurkat-HBZ and Jurkat-control, respectively) were stimulated with PMA and Io for 9 hours. Gene expression profiles were then analyzed by DNA microarray. Table 1 shows the apoptosis-associated genes that were downregulated or upregulated in stimulated Jurkat-HBZ cells. Transcription of the *Bim* gene was prominently downregulated in HBZ-expressing Jurkat cells. To confirm the effect of HBZ on the *Bim* gene expression, we evaluated *Bim* mRNA levels in Jurkat-control and Jurkat-HBZ cells with or without PMA/Io stimulation using real-time PCR. As reported in the previous studies showing that treatment by PMA/Io or other stimulators induced *Bim* expression (29, 30), the *Bim* mRNA level of stimulated Jurkat-control cells was three-times higher than that of unstimulated cells, but that of Jurkat-HBZ cells did not change after stimulation (Fig. 1A). Similarly, increased *Bim* transcription by stimulation was also inhibited by HBZ in CCRF-CEM cells (Fig. 1A).

HBZ inhibits apoptosis

It has been reported that Bim plays an important role in activation-induced cell death and T-cell homeostasis (31). Because the earlier data demonstrated that HBZ inhibits stimulation-induced *Bim* expression, we next investigated whether HBZ inhibits apoptosis in response to PMA/Io stimulation. To test this, Jurkat-control and Jurkat-HBZ were each incubated with or without PMA/Io for 9 hours, and then apoptosis was measured using Annexin V. The percentages of apoptotic cells in Jurkat-control and Jurkat-HBZ were 40.2% and 15% respectively, indicating that HBZ suppressed activation-induced apoptosis (Fig. 1B). We also treated cells with doxorubicin and found that HBZ slightly inhibited doxorubicin-induced apoptosis (Supplementary Fig. S1). Fas-mediated apoptotic pathway might be involved in antiapoptotic effect by HBZ. To assess the effect of Fas-mediated signaling on the activation-induced apoptosis, cells were also treated with or without Fas-blocking antibody (0.5 μg/mL) 30 minutes before the PMA/Io stimulation. The percentage of apoptotic cells without Fas-blocking antibody in Jurkat-control and Jurkat-HBZ were 36.9% and 22.4%, respectively. When cells were treated with Fas-blocking antibody, the percentage of apoptotic cells reduced and those were 24% and 13.2% in Jurkat-control and Jurkat-HBZ, respectively (Fig. 1C). Thus, Fas-blocking antibody partially inhibited apoptosis in Jurkat-HBZ, which indicates that Fas-mediated signals are also implicated in activation-induced cell death. Indeed, we found that the transcription level of *FasL* was suppressed in stimulated Jurkat-HBZ and CEM-HBZ cells compared with Jurkat-control and CEM-control cells (Fig. 1D), suggesting that downregulation of FasL by HBZ was also associated with inhibition of apoptosis.

Table 1. Apoptosis-associated genes that are upregulated or downregulated by HBZ

Gene	Fold change	Gene ontology
API5	2.18	Antiapoptosis
BCL2L11 (Bim)	−9.93	Induction of apoptosis
CARD11	2.87	Regulation of apoptosis
CASP1	2.97	Apoptosis
CD28	4.60	Positive regulation of antiapoptosis
COP1	9.41	Regulation of apoptosis
DEDD2	2.01	Induction of apoptosis via death domain receptors
DYRK2	2.16	Induction of apoptosis
GZMB	−5.90	Apoptosis
HIPK2	2.19	Induction of apoptosis by intracellular signals
NLRP1	3.08	Induction of apoptosis
PI3KR2	−2.68	Negative regulation of antiapoptosis
PLEKHF1	2.99	Induction of apoptosis
PRDX2	−2.10	Antiapoptosis
PRF1	3.95	Virus-infected cell apoptosis
RFFL	2.20	Apoptosis
SPHK1	−4.26	Antiapoptosis
TNFRSF9	−2.61	Induction of apoptosis
TP53INP1	2.32	Apoptosis
VEGFA	−6.96	Negative regulation of apoptosis

NOTE: The table shows a list of apoptosis-associated genes that were downregulated or upregulated (by more than 2-fold) in stimulated Jurkat-HBZ cells identified by microarray analysis.

Published OnlineFirst October 31, 2013; DOI: 10.1158/0008-5472.CAN-13-0436

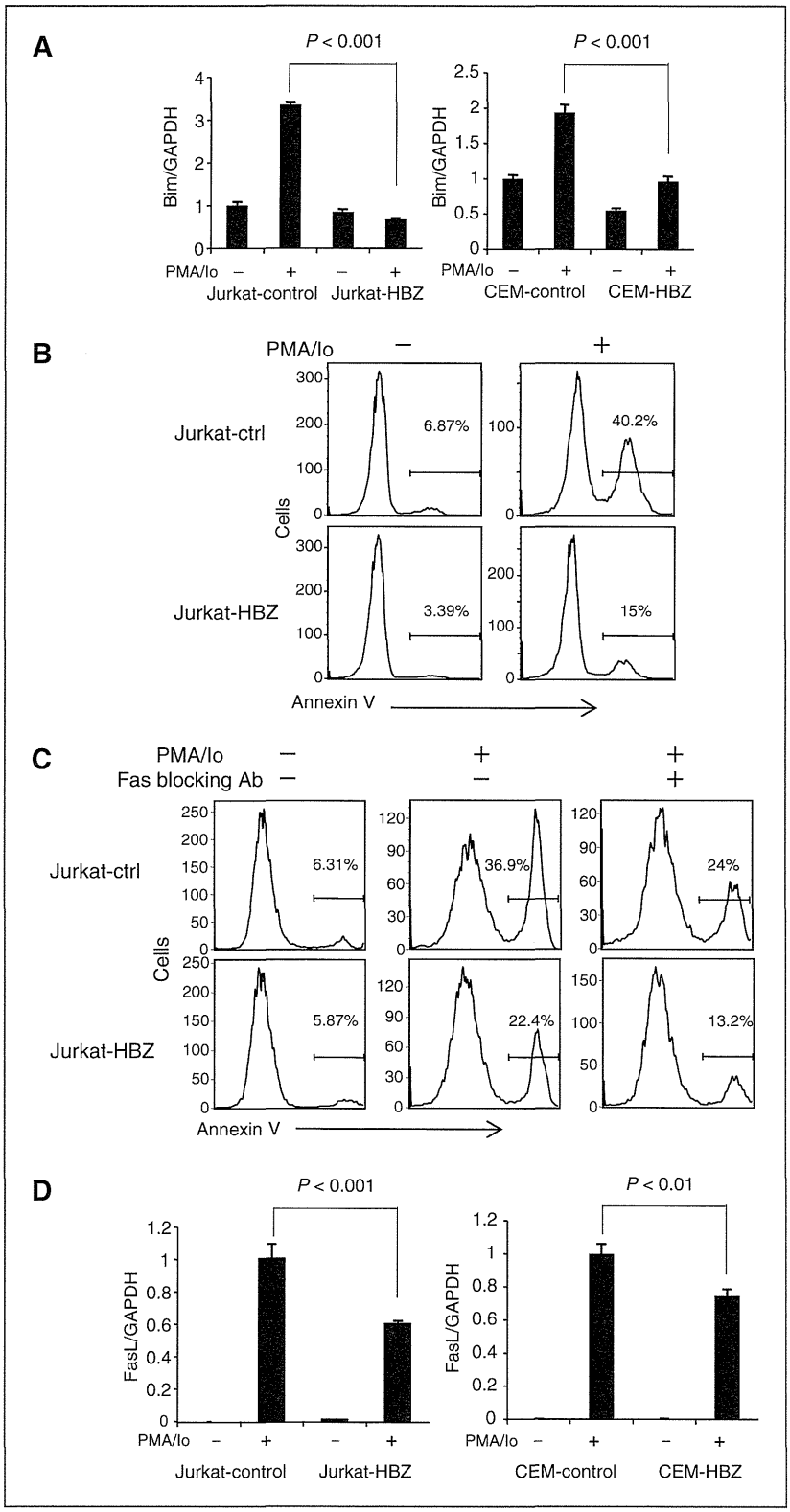

Figure 1. HBZ suppresses the transcription of the *Bim* and *FasL* genes and consequently stimulation-induced apoptosis. A, comparison of the *Bim* mRNA expression in the Jurkat-control, Jurkat-HBZ, CEM-control, and CEM-HBZ cells with or without PMA/Io stimulation by real-time PCR. B, Jurkat-control and Jurkat-HBZ were stimulated with PMA/Io for 9 hours and stained with Annexin V. Percentage of apoptotic cells was determined by flow cytometry. C, Jurkat-control and Jurkat-HBZ were treated with Fas-blocking antibody for 30 minutes and then stimulated with PMA/Io for 9 hours. Percentages of apoptotic cells were monitored by flow cytometry. D, comparison of the *FasL* mRNA transcription in the Jurkat-control, Jurkat-HBZ, CEM-control, and CEM-HBZ cells with or without PMA/Io stimulation by real-time PCR. Error bars, standard deviation. Statistical differences are calculated by Student *t* test. GAPDH, glyceraldehyde-3-phosphate dehydrogenase.

Published OnlineFirst October 31, 2013; DOI: 10.1158/0008-5472.CAN-13-0436

HBZ suppresses *Bim* expression through attenuation of FoxO3a

We analyzed how HBZ suppresses the expression of *Bim* and *FasL*. It has been reported that a forkhead factor, FoxO3a, and p73 are important for the transcription of *Bim* and *FasL* (32, 33). FoxO3a and other FOXO family members are phosphorylated by protein kinases such as Akt or SGK on highly conserved serine and threonine residues (especially Thr32, Ser253, and Ser315 in FoxO3a), resulting in impaired DNA-binding activity and increased binding to the chaperone protein, 14-3-3 (20, 34, 35). Newly formed 14-3-3-FOXO complexes are then exported from the nucleus, thereby inhibiting FOXO-dependent transcription of key target genes such as *Bim*, *FasL*, and *TRAIL* (36).

First, we investigated whether FoxO3a is implicated for the activation induced cell death. As shown in Supplementary Fig. S2, the knockdown of FoxO3a resulted in the decreased apoptotic rate in Jurkat-control cells ($P < 0.05$). Furthermore, inhibition of Foxo3a did not influence activation-induced cell death in Jurkat-HBZ cells, suggesting the inhibitory effect of HBZ on Foxo3a function. To investigate whether HBZ affects FoxO3a function, Jurkat cells were transiently transfected with a plasmid expressing FoxO3aAAA, the constitutive active mutant of FoxO3a, which is no longer phosphorylated by Akt and is localized in the nucleus. The FoxO3aAAA was expressed together with hrGFP using an internal ribosome entry site (IRES; FoxO3aAAA-IREShrGFP). Jurkat cells were transiently transfected with full-length HBZ or its mutants. HBZ has three domains, an activation domain (AD), a central domain (CD), and a basic leucine zipper domain (bZIP; ref. 12). In this study, the deletion mutants (HBZ-ΔAD, HBZ-ΔbZIP, and HBZ-ΔCD) were used. The percentage of FoxO3aAAA induced apoptotic cells in the absence of HBZ was 69.6% while it was suppressed by HBZ (40.6%; $P < 0.001$; Fig. 2A). We also found that an HBZ mutant without activation domain lacks the activity to inhibit FoxO3aAAA-induced apoptosis (Fig. 2A), indicating the significance of activation domain in suppression of FoxO3a-mediated apoptosis. It has been reported that LXXLL motif in FoxO3a binds to its coactivator CBP/p300 (37). Similarly, HBZ has LXXLL-like motifs located in the NH_2-terminal region, which bind to KIX domain of CBP/p300 (38). We speculated that the LXXLL-like motifs of HBZ might affect FoxO3aAAA function through KIX domain of CBP/p300. An HBZ mutant, which has substitutions in 27th and 28th residues (LL to AA) of LXXLL-like motif, lack the activity to suppress FoxO3aAAA-mediated apoptosis (Fig. 2B), indicating that LXXLL-like motif of HBZ is critical for suppression of FoxO3a-mediated apoptosis.

Next, we analyzed the effect of HBZ on a FoxO3a responsive reporter. As shown in Fig. 2C, HBZ suppressed FoxO3a-mediated transcriptional activity ($P < 0.01$). To check whether HBZ inhibits DNA binding of FoxO3a, 293T cells were transiently transfected with FoxO3aAAA and FoxO3a reporter, 6xDBE-Luc, together with or without HBZ. The interaction of FoxO3aAAA to FOXO-binding sites was analyzed by ChIP assay. As shown in Figure 2D, the interaction of FoxO3aAAA to the FOXO-binding sites was interfered by HBZ, suggesting that HBZ inhibits FoxO3a-mediated apoptosis through suppression of the DNA binding of FoxO3a. To clarify the mechanism of HBZ-mediated FoxO3a inhibition, we examined interaction between HBZ and FoxO3a by the immunoprecipitation assay. It showed that HBZ interacted with FoxO3a (Fig. 2E and F). Experiments with FoxO3a deletion mutant revealed that HBZ interacted with the forkhead domain of FoxO3a (Fig. 2E). Analysis using HBZ deletion mutants showed that the central domain of HBZ interacted with FoxO3a (Fig. 2F).

HBZ inhibits nuclear export of phosphorylated form of FoxO3a

Next, we investigated the effect of HBZ on FoxO3a localization by confocal microscopy. We cotransfected 293FT cells with a plasmid expressing human wild-type FoxO3a (FoxO3aWT) protein and an HBZ-expressing plasmid. Consistent with previous reports, FoxO3a remained mainly in cytoplasm when cells were cotransfected with empty vector (Fig. 3A; refs. 20, 34). However, when it was expressed along with HBZ, FoxO3a was localized in both nucleus and cytoplasm (Fig. 3A). To determine whether mislocalized FoxO3a is phosphorylated (pFoxO3a) or not, we used anti-pFoxO3a antibody. Figure 3B and C demonstrated that nuclear-localized FoxO3a was phosphorylated in HBZ-expressing cells. Thereafter, we analyzed the localization of endogenous FoxO3a in HeLa and an ATL cell line, MT-1. Although pFoxO3a was localized widely both in cytoplasm and nucleus in HeLa cells, most pFoxO3a was localized in the nucleus in MT-1 (Fig. 3D), suggesting that endogenous HBZ inhibits the extranuclear translocation of pFoxO3a in this cell line. From the study of crystal structure of the human FoxO3a-DBD/DNA complex, it has been reported that phosphorylation at Ser253 causes a decrease on the DNA-binding ability (39). Abnormal localization of phosphorylated FoxO3a by HBZ might interfere the function of unphosphorylated FoxO3a in the nucleus. The abnormal localization of pFoxO3a prompted us to investigate whether HBZ bound to 14-3-3 along with FoxO3a, as 14-3-3 is a chaperon protein involved in nuclear–cytoplasm shuttling of FOXO family. As shown in Figure 3E, HBZ, FoxO3a, and 14-3-3 form a ternary complex. However, the binding of FoxO3a and 14-3-3 was not affected by HBZ (result of IP with anti-FLAG antibody and detected with anti-HA antibody).

As another possible mechanism for downregulation of *Bim* and *FasL*, we compared the transcription level of *p73* in Jurkat cells with and without HBZ expression. Activation of HBZ-expressing cells reduced transcription of *p73*, but the expression level of *p73* was variable among ATL cell lines (Supplementary Fig. S3A and S3B). We conclude that p73 is not responsible for suppression of *Bim* expression in ATL cells.

Bim expression is suppressed in both ATL cell lines and ATL cases

HBZ has been shown to suppress Bim expression through two different mechanisms as revealed in this study. To analyze Bim expression in ATL cells, we studied *Bim* mRNA levels in non-ATL cell lines and ATL cell lines with or without PMA/Io stimulation, and found that the *Bim* gene transcript was upregulated in Jurkat and CCRF-CEM cells, but not in SupT1 after activation. However, *Bim* transcripts were not increased

Published OnlineFirst October 31, 2013; DOI: 10.1158/0008-5472.CAN-13-0436

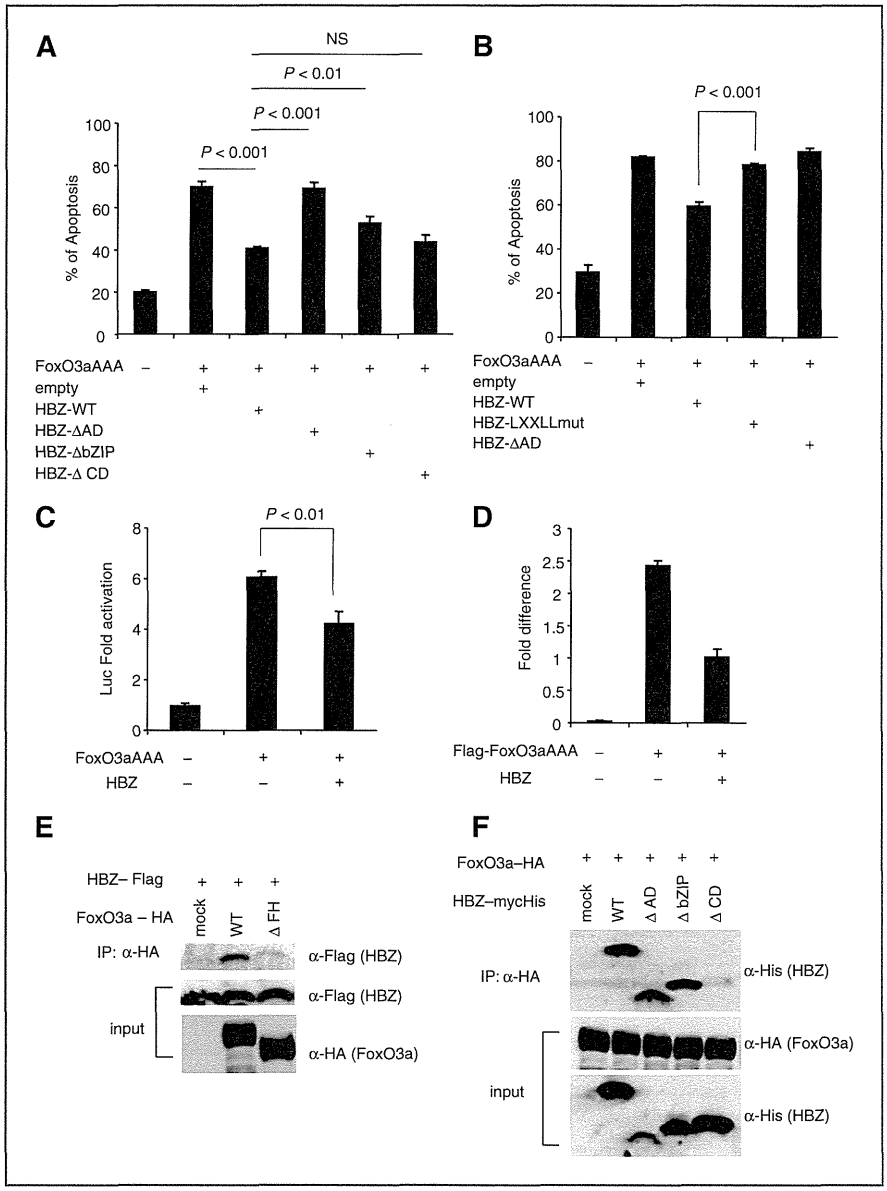

Figure 2. HBZ attenuates function of Foxo3a by physical interaction. A, Jurkat cells were transfected with FoxO3aAAA-expressing vector, a constitutively active form, by using Neon with or without HBZ or its mutants. Twenty-four hours after transfection, cells were stained with Annexin V and analyzed by flow cytometry ($n = 3$). B, Jurkat cells were transfected with FoxO3aAAA-expressing vector together with HBZ or its mutants by using Neon. Cells were stained with Annexin V and analyzed by flow cytometry ($n = 3$). Data are representative of three independent experiments. C, reporter construct containing the 6xDBE and FoxO3aAAA-expressing vector was transiently transfected with or without HBZ into Jurkat cells in the presence of Z-VAD-FMK and luciferase activities were measured. D, 293T cells were transfected with 6xDBE-Luc construct and Flag-tagged FoxO3aAAA expression vector together with or without HBZ expression vector. Cells were immunoprecipitated with anti-FLAG antibody and quantified by real-time PCR. Three independent ChIP experiments were done and representative data are shown. Error bars, experimental variation. E and F, the expression vectors of the indicated proteins were cotransfected into 293T cells, and their interactions were analyzed by immunoprecipitation assay. Data are representative of three independent experiments. Statistical differences are calculated by Student *t* test.

in all stimulated ATL cell lines (Fig. 4A). The *Bim* gene transcript was also downregulated in primary ATL cells (Fig. 4B) compared with resting peripheral blood mononuclear cells (PBMC) and phytohemagglutinin (PHA)-stimulated T cells. We also stimulated primary ATL cells and normal $CD4^+$ T cells with PMA/Io. The *Bim* gene transcription was quite low in primary ATL sample compared with normal $CD4^+$ T cells even though the cells were stimulated with PMA/Io (Fig. 4C). To confirm HBZ expression in representative ATL cell lines, we quantified the level of the *HBZ* mRNA transcription in Jurkat-HBZ, CEM-HBZ, MT-1, ED, and TL-Om1 by real-time PCR and confirmed that HBZ is expressed in these ATL cell lines (Supplementary Fig. S4). Microarray data, obtained from Gene Expression Omnibus (GEO), show that both *Bim* and *FasL* transcription levels are lower in ATL cases than healthy donors (accession number: GSE33615; Supplementary Fig. S5), supporting our data that *Bim* expression was suppressed in ATL cells.

Bim expression is silenced by epigenetic mechanisms

Because the *Bim* gene transcription was severely suppressed in ATL cells, we investigated the epigenetic status (DNA methylation and histone modification) of the promoter region of the *Bim* gene in ATL cells. A previous study showed that the 0.8 kb region immediately upstream of exon 1 contains the important elements for the control of *Bim* expression

Published OnlineFirst October 31, 2013; DOI: 10.1158/0008-5472.CAN-13-0436

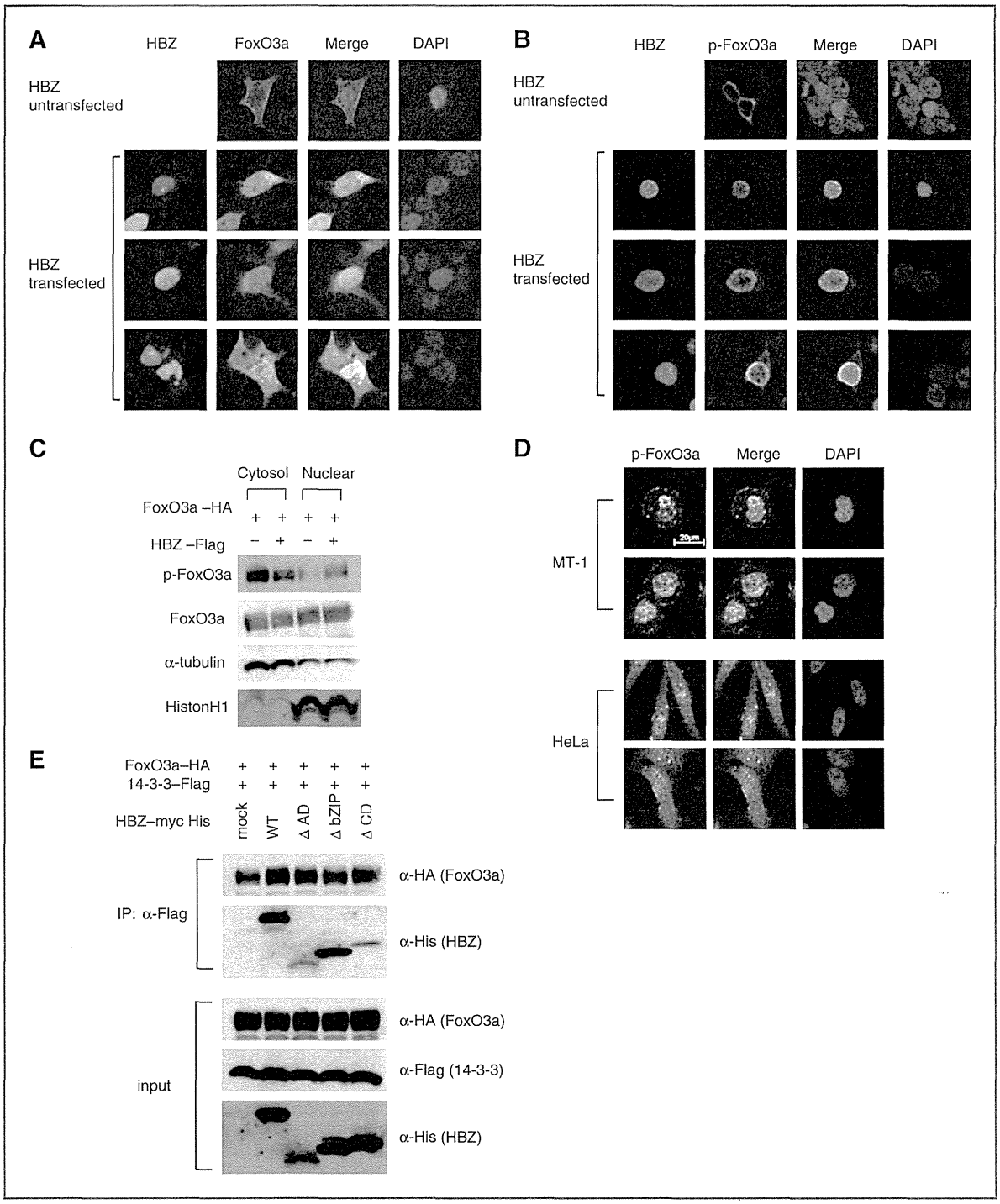

Figure 3. HBZ interferes with normal localization of FoxO3a by forming a ternary complex with FoxO3a and 14-3-3. 293FT cells were transfected with FoxO3aWT-Flag together with or without mycHis-HBZ. A and B, FoxO3a was detected using anti-FLAG-biotin and secondary Streptavidin-Alexa 488 (A), and p-FoxO3a was detected using anti-p-FoxO3a (ser253) and secondary anti-rabbit IgG-Alexa 488 antibody (B). DAPI was used to counterstain the nucleus. C, 293FT cells were transfected with HA-tagged FoxO3aWT together with or without Flag-tagged HBZ. Cytoplasmatic and nuclear fractions were extracted and p-FoxO3a was detected by Western-blotting. D, endogenous localizations of p-FoxO3a (ser253) in HeLa and MT-1 cells were examined using anti-p-FoxO3a. E, the interactions among HBZ, FoxO3a, and 14-3-3 were analyzed by immunoprecipitation.

Published OnlineFirst October 31, 2013; DOI: 10.1158/0008-5472.CAN-13-0436

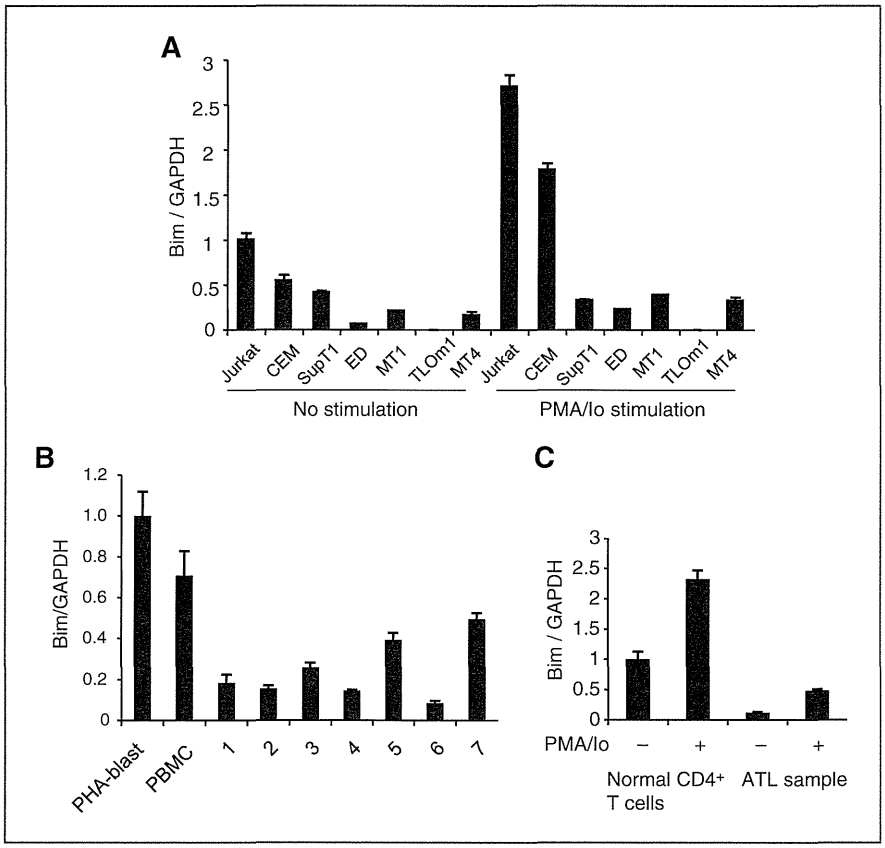

Figure 4. Bim expression is also suppressed in ATL cell lines and ATL cases. Comparison of the *Bim* mRNA expression in non-ATL cell lines and ATL cell lines with or without PMA/Io stimulation (A) and in PBMCs and PHA-blasts from healthy donor samples and fresh ATL samples (B) by real-time PCR. C, comparison of the *Bim* mRNA expression in healthy donor sample and ATL fresh sample with or without PMA/Io stimulation.

(promoter 1). The *Bim* promoter does not contain a TATA or CAAT box and has the characteristics of a "TATA-less" promoter (40). In addition, the alternative promoter has been reported to exist in intron 1 (promoter 2; refs. 41, 42). These two promoter regions are highly GC-rich and contain the binding sites for several transcription factors, including FoxO3a. To determine whether CpG sites in these *Bim* gene promoter regions are methylated in ATL cell lines, their methylation status was analyzed by bisulfite-mediated methylcytosine mapping (Supplementary Fig. S6A and S6B). The promoter 1 of *Bim* was hypermethylated in two ATL cell lines (ED and TL-Om1) and ATL case 1, whereas this region was not so methylated in MT-1 cells and two ATL cases. On the other hand, the promoter 2 was heavily methylated in two ATL cell lines (TL-Om1 and MT-1) and ATL case 1 and partially methylated in Jurkat cells (Supplementary Fig. S6B). These results suggest that in some cases, heavily methylated CpG sites of promoter 1 and 2 are associated with silencing of *Bim* transcription but these methylations can not account for suppressed *Bim* expression in all ATL cell lines and ATL cases.

Therefore, we next focused on the histone modification in the promoter region of *Bim*. It is well known that deacetylation of the histones are also common features of cancer, which results in transcriptional silencing of tumor suppressor genes (43). First, we analyzed the histone H3 and H4 acetylation and H3K4 trimethylation, which are all permissive marks (44), in promoter 1 of Jurkat, MT-1, and TL-Om1 cells. Contrary to our speculation, neither H3, H4 acetylation, nor H3K4 trimethylation differed between MT-1 and Jurkat cells (Supplementary Fig. S7). We next analyzed the histone modification status in promoter 2. As shown in Figure 5A, MT-1 and TL-Om1 cells exhibited decreased level of histone H3 acetylation and H3K4 trimethylation but not histone H4 acetylation. Because methylation of DNA is often preceded by dimethylation of H3K9 or trimethylation of H3K27 (both repressive marks) in oncogenesis (44), we asked whether there were differences in these epigenetic chromatin marks on the *Bim* gene promoter in ATL cell lines. TL-Om1 cells exhibited upregulated level of H3K9 dimethylation and H3K27 trimethylation compared with Jurkat cells (Fig. 5B and C), whereas MT-1 exhibited a little upregulated level of H3K27 trimethylation (Fig. 5C) in the promoter 2. These data suggest that histone modifications of promoter 2 are critical for the suppressed *Bim* gene transcription. We also performed ChIP analysis using anti-RNA polymerase II antibody (Fig. 5D) and revealed that Pol II binding was decreased in MT-1 and TL-Om1 cells, confirming suppressed transcription of the *Bim* gene. To further investigate the mechanisms involved in FoxO3a-mediated *Bim* gene transcription in the promoter 2, we transfected HA-tagged FoxO3a expression vector together with or without a HBZ expression vector into 293T cells and immunoprecipitated with anti-HA antibody. Then, the DNA-binding capacity of FoxO3a was

Published OnlineFirst October 31, 2013; DOI: 10.1158/0008-5472.CAN-13-0436

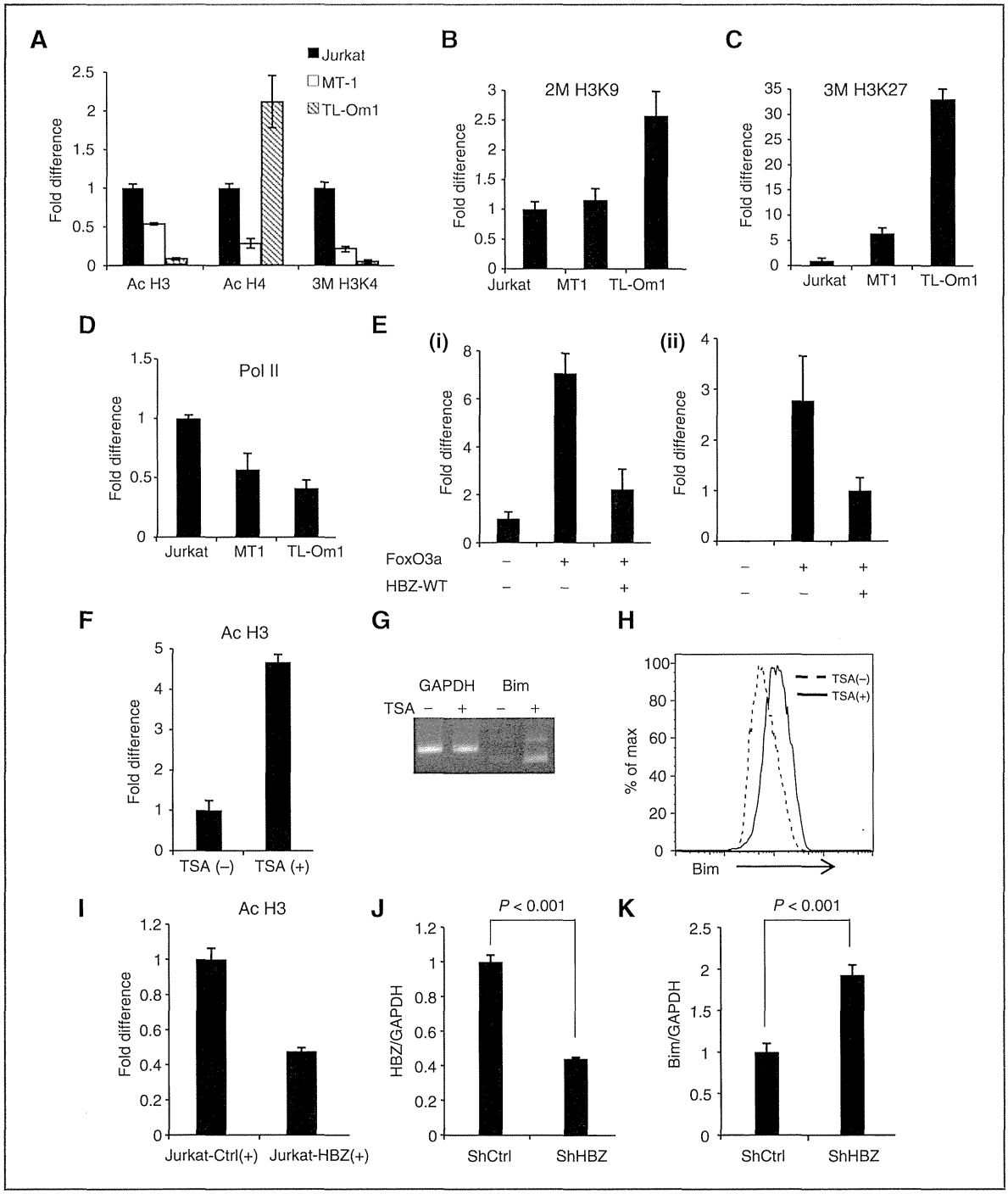

Figure 5. Epigenetic status of the promoter regions of the *Bim* gene. A–C, fold difference of acetylated histone H3, acetylated histone H4, trimethylated H3K4, dimethylated H3K9, or trimethylated H3K27; the data from Jurkat cells were arbitrarily set as 1.0. D, quantitative ChIP assay using RNA polymerase II (Pol II) antibody in Jurkat, MT-1, and TL-Om1 cells. E, 293T cells were transfected with HA-tagged FoxO3a expression vector together with or without HBZ expression vector. Cells were immunoprecipitated with anti-HA antibody and DNA-binding ability at promoter 2 was quantified by real-time PCR. F, fold difference of acetylated histone H3 in MT-1 cells, which were treated with or without 0.4 mmol/L TSA for 15 hours. The data from MT-1 cells without TSA treatment were arbitrarily set as 1.0. G and H, MT-1 cells were treated with 0.4 mmol/L TSA for 15 hours and *Bim* expression level was analyzed by quantitative real-time PCR and flow cytometry. I, fold difference of acetylated histone H3 in the Bim promoter in the Jurkat-control and Jurkat-HBZ cells 9 hours after the stimulation with PMA/Io. J, HBZ transcript in shRNA transfectant of MT-1 was quantified by real-time PCR. K, comparison of the *Bim* mRNA expression in control MT-1 cells and HBZ-KD MT-1 cells. Error bars, experimental variation. The data shown are representative of two or three independent experiments. Statistical differences are calculated by Student *t* test. GAPDH, glyceraldehyde-3-phosphate dehydrogenase.

Published OnlineFirst October 31, 2013; DOI: 10.1158/0008-5472.CAN-13-0436

quantified by real-time PCR. Figure 5E shows that HBZ attenuated the DNA-binding capacity of FoxO3a in the promoter 2 of *Bim* (i) and *FasL* promoter (ii), suggesting that the suppressed binding of FoxO3a to the promoter regions leads to inhibition of the *Bim* and *FasL* genes transcription by HBZ.

Next, we treated MT-1 cells with trichostatin A (TSA), a cell-permeable chemical inhibitor of class I/II histone deacetylases (HDAC). Treatment of TSA resulted in a clear upregulation of acetylation of histone H3 (Fig. 5F) followed by Bim expression both at the mRNA (Fig. 5G) and protein levels (Fig. 5H), indicating that histone modification is associated with suppressed *Bim* transcription in MT-1. We also performed ChIP assay using Jurkat-control and Jurkat-HBZ cells, which were stimulated with PMA and ionomycin for 9 hours, and found that acetylation of histone H3 decreased in Jurkat-HBZ cells (Fig. 5I), suggesting that HBZ is implicated in histone deacetylation in T cells. To verify whether HBZ inhibits transcription of the *Bim* gene, we suppressed the *HBZ* gene transcription by shRNA as reported previously (11). Efficiencies of lentivirus vector transduction, which were determined by EGFP expression, were 90.5% and 90.3% for control MT-1 cells and HBZ-knockdown MT-1 cells, respectively. Suppressed HBZ expression led to increase the *Bim* gene transcription (Fig. 5J and K), indicating that HBZ expression is linked to suppression of *Bim* expression in ATL cells.

Discussion

Human immunodeficiency virus type 1 (HIV-1) replicates vigorously and the generated virus infects target cells *in vivo*. Unlike HIV-1, HTLV-1 induces proliferation to increase the number of infected cells, as this virus is transmitted primarily by cell-to-cell contact (5). Therefore, HTLV-1–encoded proteins promote proliferation of infected cells and inhibit their apoptosis, resulting in an increased number of infected cells *in vivo* (2). In this study, we show that HBZ inhibits both the intrinsic and extrinsic apoptotic pathways via targeting FoxO3a, which leads to suppressed transcriptions of *Bim* and *FasL*. We demonstrated two mechanisms for perturbation of FoxO3a by HBZ: interaction of HBZ with FoxO3a and interference of nuclear export of phosphorylated FoxO3a. HBZ suppresses DNA-binding ability of active form of FoxO3a through interaction between central domain of HBZ and forkhead domain of FoxO3a. In addition, LXXLL-like motif of HBZ is implicated in inhibition of FoxO3a-mediated apoptosis, suggesting that HBZ interferes in interaction of CBP/p300 and FoxO3a. Furthermore, HBZ retains inactive form of FoxO3a in the nucleus through interaction with 14-3-3, leading to transcriptional repression of the target genes. Interestingly, accumulation of phosphorylated form of FoxO3a in the nucleus has been observed in HIV Vpr-expressing cells, which might be implicated in HIV-mediated resistance against insulin (28). Thus, FoxO3a is a target of both human retroviruses.

In this study, we showed that central domain of HBZ interacts with FoxO3a while LXXLL-like motif in activation domain of HBZ is responsible for suppressed apoptosis. LXXLL-like motif of HBZ has been reported to interact with KIX domain of p300 (38). The central domain of HBZ interacts with the forkhead domain of FoxO3a, which binds to the target sequence (35). This is the mechanism how HBZ inhibits DNA binding of FoxO3a. However, inhibitory effect of HBZ on apoptosis largely depends on LXXLL-like motif of activation domain (Fig. 2A and B). FoxO3a is also reported to interact with KIX domain of CBP/p300 (37). Forkhead domain of FoxO3a intramolecularly interacts with its conserved regions (CR) 3, and binding of forkhead domain to DNA releases CR3, allowing it to bind KIX of CBP/p300 (45). These findings suggest that HBZ interferes in the complex interaction between FoxO3a and CBP/p300, which is likely important to induce apoptosis.

It has been reported that Bim has a tumor-suppressor function in various cancers. Hemizygous loss of the *Bim* gene promoted development of B-cell leukemia in Myc-transgenic mice in which c-myc expression was driven by the immunoglobulin gene intron-enhancer (46). Insulin-like growth factor 1 (IGF-1), an important growth factor for myeloma cells, has been reported to suppress Bim expression by epigenetic and posttranslational mechanisms (25). In Epstein–Barr virus–infected B cells, *Bim* transcription is silenced by DNA methylation of the *Bim* gene promoter (47). Thus, impaired expression of Bim is associated with the various cancers, including the virus-related malignancies. FoxO3a is also a target of oncogenesis. BCR-ABL induces phosphorylation of FoxO3a, which leads to suppressed expression of Bim in $Ph1^+$ chronic myelogenous leukemia cells (32). In breast cancer, IκB kinase interacts with, phosphorylates FoxO3a, which causes proteolysis of FoxO3a (48). In this study, we revealed that HBZ hinders nuclear export of phosphorylated FoxO3a, and impairs function of FoxO3a likely through interaction of FoxO3a and p300. Thus, suppressed Bim and FasL expression through inhibition of FoxO3a by HBZ is a new mechanism for oncogenesis.

Besides FoxO3a perturbation by HBZ, we also have identified the epigenetic aberrations in the promoter region of the *Bim* gene in ATL cells, and found that Bim expression is suppressed by DNA methylation and histone modification. ATL cell lines exhibited upregulated level of H3K27 trimethylation in the promoter regions of *Bim*. It has been reported that enhancer of zeste (EZH) 2, a methyltransferase and component of the polycomb repressive complex 2, expression is increased in ATL cell lines (42). Because EZH2 plays an essential role in the epigenetic maintenance of H3K27 trimethylation, upregulated H3K27 trimethylation of the *Bim* gene promoter might be associated with increased expression of EZH2 in ATL cells. In addition, HBZ seems to be associated with histone deacetylation in MT-1 cells. According to the previous studies, it is known that both HBZ and FoxO3a bind to the histone acetyltransferase p300/CBP through the LXXLL motif (38). In this study, we found that the same motif is important for FoxO3a suppression and resulting inhibition of apoptosis. It is likely that HBZ decreases histone acetylation level on Bim promoter through the interaction with FoxO3a and dissociation of p300/CBP from the promoter. In addition to histone modifications, hypermethylation of CpGs in Bim promoter was observed in some ATL cells. These epigenetic aberrations likely occur as the secondary changes following long-time silencing of *Bim* by HBZ, although further investigations will be required.

Published OnlineFirst October 31, 2013; DOI: 10.1158/0008-5472.CAN-13-0436

In this study, we demonstrated that HBZ suppresses activation-induced apoptosis by downregulation of proapoptotic genes, *Bim* and *FasL*. HBZ perturbs the function of FoxO3a by interaction, and induces epigenetic aberrations in the promoter region of the *Bim* gene. It has been shown that HBZ induces not only cancer but also inflammation *in vivo*. Because inflammatory diseases are essentially caused by failure to negatively regulate unnecessary immune responses by apoptosis, suppression of apoptosis by HBZ might be associated with HTLV-1–induced inflammation as well. Collectively, HBZ-mediated inhibition of apoptosis is likely implicated in both neoplastic and inflammatory diseases caused by HTLV-1.

Disclosure of Potential Conflicts of Interest

No potential conflicts of interest were disclosed.

Authors' Contributions

Conception and design: A. Tanaka-Nakanishi, J. Yasunaga, M. Matsuoka
Development of methodology: A. Tanaka-Nakanishi, M. Matsuoka
Acquisition of data (provided animals, acquired and managed patients, provided facilities, etc.): A. Tanaka-Nakanishi, K. Takai
Analysis and interpretation of data (e.g., statistical analysis, biostatistics, computational analysis): A. Tanaka-Nakanishi, J. Yasunaga, K. Takai, M. Matsuoka
Writing, review, and/or revision of the manuscript: A. Tanaka-Nakanishi, J. Yasunaga, M. Matsuoka
Administrative, technical, or material support (i.e., reporting or organizing data, constructing databases): M. Matsuoka
Study supervision: M. Matsuoka

Acknowledgments

The authors thank T. Furuyama (Kagawa Prefectural University of Health Science) for the 6xDBE-Luc plasmid DNA, P. Bouillet for valuable comments on this study, and L. Kingsbury for proofreading of this manuscript.

Grant Support

This study was supported by a Grant-in-aid for Scientific Research from the Ministry of Education, Science, Sports, and Culture of Japan to M. Matsuoka (MEXT grant number 221S0001), a grant from Japan Leukemia Research Fund to M. Matsuoka, and a grant from the Takeda Science Foundation to J. Yasunaga.

The costs of publication of this article were defrayed in part by the payment of page charges. This article must therefore be hereby marked *advertisement* in accordance with 18 U.S.C. Section 1734 solely to indicate this fact.

Received February 14, 2013; revised September 12, 2013; accepted October 5, 2013; published OnlineFirst October 31, 2013.

References

1. Proietti FA, Carneiro-Proietti AB, Catalan-Soares BC, Murphy EL. Global epidemiology of HTLV-I infection and associated diseases. Oncogene 2005;24:6058–68.
2. Matsuoka M, Jeang KT. Human T-cell leukaemia virus type 1 (HTLV-1) *infectivity and cellular transformation*. Nat Rev *Cancer* 2007;7:270–80.
3. Igakura T, Stinchcombe JC, Goon PK, Taylor GP, Weber JN, Griffiths GM, et al. Spread of HTLV-I between lymphocytes by virus-induced polarization of the cytoskeleton. Science 2003;299:1713–6.
4. Pais-Correia AM, Sachse M, Guadagnini S, Robbiati V, Lasserre R, Gessain A, et al. Biofilm-like extracellular viral assemblies mediate HTLV-1 cell-to-cell transmission at virological synapses. Nat Med 2010;16:83–9.
5. Derse D, Hill SA, Lloyd PA, Chung H, Morse BA. Examining human T-lymphotropic virus type 1 infection and replication by cell-free infection with recombinant virus vectors. J Virol 2001;75:8461–8.
6. Mazurov D, Ilinskaya A, Heidecker G, Lloyd P, Derse D. Quantitative comparison of HTLV-1 and HIV-1 cell-to-cell infection with new replication dependent vectors. PLoS Pathog 2010;6:e1000788.
7. Cavrois M, Leclercq I, Gout O, Gessain A, Wain-Hobson S, Wattel E. Persistent oligoclonal expansion of human T-cell leukemia virus type 1-infected circulating cells in patients with Tropical spastic paraparesis/HTLV-1 associated myelopathy. Oncogene 1998;17:77–82.
8. Etoh K, Tamiya S, Yamaguchi K, Okayama A, Tsubouchi H, Ideta T, et al. Persistent clonal proliferation of human T-lymphotropic virus type I-infected cells *in vivo*. Cancer Res 1997;57:4862–7.
9. Grassmann R, Aboud M, Jeang KT. Molecular mechanisms of cellular transformation by HTLV-1 Tax. Oncogene 2005;24:5976–85.
10. Fan J, Ma G, Nosaka K, Tanabe J, Satou Y, Koito A, et al. APOBEC3G generates nonsense mutations in HTLV-1 proviral genomes *in vivo*. J Virol 2010;84:7278–87.
11. Satou Y, Yasunaga J, Yoshida M, Matsuoka M. HTLV-I basic leucine zipper factor gene mRNA supports proliferation of adult T cell leukemia cells. Proc Natl Acad Sci U S A 2006;103:720–5.
12. Satou Y, Yasunaga J, Zhao T, Yoshida M, Miyazato P, Takai K, et al. HTLV-1 bZIP factor induces T-cell lymphoma and systemic inflammation *in vivo*. PLoS Pathog 2011;7:e1001274.
13. Bouillet P, O'Reilly LA. CD95, BIM and T cell homeostasis. Nat Rev Immunol 2009;9:514–9.
14. Debatin KM, Goldman CK, Waldmann TA, Krammer PH. APO-1-induced apoptosis of leukemia cells from patients with adult T-cell leukemia. Blood 1993;81:2972–7.
15. Yasunaga J, Taniguchi Y, Nosaka K, Yoshida M, Satou Y, Sakai T, et al. Identification of aberrantly methylated genes in association with adult T-cell leukemia. Cancer Res 2004;64:6002–9.
16. Krueger A, Fas SC, Giaisi M, Bleumink M, Merling A, Stumpf C, et al. *HTLV-1 Tax protects against CD95-mediated apoptosis by induction* of the cellular FLICE-inhibitory protein (c-FLIP). Blood 2006;107:3933–9.
17. Okamoto K, Fujisawa J, Reth M, Yonehara S. Human T-cell leukemia virus type-I oncoprotein Tax inhibits Fas-mediated apoptosis by inducing cellular FLIP through activation of NF-kappaB. Genes Cells 2006;11:177–91.
18. Sun SC, Yamaoka S. Activation of NF-kappaB by HTLV-I and implications for cell transformation. Oncogene 2005;24:5952–64.
19. Zhao T, Yasunaga J, Satou Y, Nakao M, Takahashi M, Fujii M, et al. Human T-cell leukemia virus type 1 bZIP factor selectively suppresses the classical pathway of NF-kappaB. Blood 2009;113:2755–64.
20. Brunet A, Bonni A, Zigmond MJ, Lin MZ, Juo P, Hu LS, et al. Akt promotes cell survival by phosphorylating and inhibiting a Forkhead transcription factor. Cell 1999;96:857–68.
21. Zhao T, Satou Y, Sugata K, Miyazato P, Green PL, Imamura T, et al. HTLV-1 bZIP factor enhances TGF-{beta} signaling through p300 coactivator. Blood 2011;118:1865–76.
22. Furuyama T, Nakazawa T, Nakano I, Mori N. Identification of the *differential distribution patterns of mRNAs and consensus binding* sequences for mouse DAF-16 homologues. Biochem J 2000;349:629–34.
23. Ponchel F, Toomes C, Bransfield K, Leong FT, Douglas SH, Field SL, et al. Real-time PCR based on SYBR-Green I fluorescence: an alternative to the TaqMan assay for a relative quantification of gene rearrangements, gene amplifications and micro gene deletions. BMC Biotechnol 2003;3:18.
24. Richter-Larrea JA, Robles EF, Fresquet V, Beltran E, Rullan AJ, Agirre X, et al. Reversion of epigenetically mediated BIM silencing overcomes chemoresistance in Burkitt lymphoma. Blood 2010;116:2531–42.
25. De Bruyne E, Bos TJ, Schuit F, Van Valckenborgh E, Menu E, Thorrez L, et al. IGF-1 suppresses Bim expression in multiple myeloma via epigenetic and posttranslational mechanisms. Blood 2010;115:2430–40.
26. Fan J, Kodama E, Koh Y, Nakao M, Matsuoka M. Halogenated thymidine analogues restore the expression of silenced genes without demethylation. Cancer Res 2005;65:6927–33.

Published OnlineFirst October 31, 2013; DOI: 10.1158/0008-5472.CAN-13-0436

27. Kumaki Y, Oda M, Okano M. QUMA: quantification tool for methylation analysis. Nucleic Acids Res 2008;36:W170–5.
28. Kino T, De Martino MU, Charmandari E, Ichijo T, Outas T, Chrousos GP. HIV-1 accessory protein Vpr inhibits the effect of insulin on the Foxo subfamily of forkhead transcription factors by interfering with their binding to 14-3-3 proteins: potential clinical implications regarding the insulin resistance of HIV-1-infected patients. Diabetes 2005;54:23–31.
29. Cante-Barrett K, Gallo EM, Winslow MM, Crabtree GR. Thymocyte negative selection is mediated by protein kinase C- and Ca2+-dependent transcriptional induction of bim [corrected]. J Immunol 2006;176:2299–306.
30. Snow AL, Oliveira JB, Zheng L, Dale JK, Fleisher TA, Lenardo MJ. Critical role for BIM in T cell receptor restimulation-induced death. Biol Direct 2008;3:34.
31. Green DR, Droin N, Pinkoski M. Activation-induced cell death in T cells. Immunol Rev 2003;193:70–81.
32. Essafi A, Fernandez de Mattos S, Hassen YA, Soeiro I, Mufti GJ, Thomas NS, et al. Direct transcriptional regulation of Bim by FoxO3a mediates STI571-induced apoptosis in Bcr-Abl-expressing cells. Oncogene 2005;24:2317–29.
33. Busuttil V, Droin N, McCormick L, Bernassola F, Candi E, Melino G, et al. NF-kappaB inhibits T-cell activation-induced, p73-dependent cell death by induction of MDM2. Proc Natl Acad Sci U S A 2010;107:18061–6.
34. Brunet A, Park J, Tran H, Hu LS, Hemmings BA, Greenberg ME. Protein kinase SGK mediates survival signals by phosphorylating the forkhead transcription factor FKHRL1 (FOXO3a). Mol Cell Biol 2001;21:952–65.
35. Obsil T, Obsilova V. Structure/function relationships underlying regulation of FOXO transcription factors. Oncogene 2008;27:2263–75.
36. Modur V, Nagarajan R, Evers BM, Milbrandt J. FOXO proteins regulate tumor necrosis factor-related apoptosis inducing ligand expression. Implications for PTEN mutation in prostate cancer. J Biol Chem 2002;277:47928–37.
37. Wang F, Marshall CB, Yamamoto K, Li GY, Gasmi-Seabrook GM, Okada H, et al. Structures of KIX domain of CBP in complex with two FOXO3a transactivation domains reveal promiscuity and plasticity in coactivator recruitment. Proc Natl Acad Sci U S A 2012;109:6078–83.
38. Clerc I, Polakowski N, Andre-Arpin C, Cook P, Barbeau B, Mesnard JM, et al. An interaction between the human T cell leukemia virus type 1 basic leucine zipper factor (HBZ) and the KIX domain of p300/CBP contributes to the down-regulation of tax-dependent viral transcription by HBZ. J Biol Chem 2008;283:23903–13.
39. Tsai KL, Sun YJ, Huang CY, Yang JY, Hung MC, Hsiao CD. Crystal structure of the human FOXO3a-DBD/DNA complex suggests the effects of post-translational modification. Nucleic Acids Res 2007;35:6984–94.
40. Bouillet P, Zhang LC, Huang DC, Webb GC, Bottema CD, Shore P, et al. Gene structure alternative splicing, and chromosomal localization of pro-apoptotic Bcl-2 relative Bim. Mamm Genome 2001;12:163–8.
41. Gilley J, Ham J. Evidence for increased complexity in the regulation of Bim expression in sympathetic neurons: involvement of novel transcriptional and translational mechanisms. DNA Cell Biol 2005;24:563–73.
42. Gilley J, Coffer PJ, Ham J. FOXO transcription factors directly activate bim gene expression and promote apoptosis in sympathetic neurons. J Cell Biol 2003;162:613–22.
43. Marks P, Rifkind RA, Richon VM, Breslow R, Miller T, Kelly WK. Histone deacetylases and cancer: causes and therapies. Nat Rev Cancer 2001;1:194–202.
44. Fullgrabe J, Kavanagh E, Joseph B. Histone onco-modifications. Oncogene 2011;30:3391–403.
45. Wang F, Marshall CB, Li GY, Yamamoto K, Mak TW, Ikura M. Synergistic interplay between promoter recognition and CBP/p300 coactivator recruitment by FOXO3a. ACS Chem Biol 2009;4:1017–27.
46. Egle A, Harris AW, Bouillet P, Cory S. Bim is a suppressor of Myc-induced mouse B cell leukemia. Proc Natl Acad Sci U S A 2004;101:6164–9.
47. Paschos K, Smith P, Anderton E, Middeldorp JM, White RE, Allday MJ. Epstein-barr virus latency in B cells leads to epigenetic repression and CpG methylation of the tumour suppressor gene Bim. PLoS Pathog 2009;5:e1000492.
48. Hu MC, Lee DF, Xia W, Golfman LS, Ou-Yang F, Yang JY, et al. IkappaB kinase promotes tumorigenesis through inhibition of forkhead FOXO3a. Cell 2004;117:225–37.

Published OnlineFirst October 31, 2013; DOI: 10.1158/0008-5472.CAN-13-0436

AACR American Association for Cancer Research

Cancer Research

The Journal of Cancer Research (1916–1930) | The American Journal of Cancer (1931–1940)

HTLV-1 bZIP Factor Suppresses Apoptosis by Attenuating the Function of FoxO3a and Altering Its Localization

Azusa Tanaka-Nakanishi, Jun-ichirou Yasunaga, Ken Takai, et al.

Cancer Res 2014;74:188-200. Published OnlineFirst October 31, 2013.

VOLUME 32 · NUMBER 11 · APRIL 10 2014

JOURNAL OF CLINICAL ONCOLOGY

ORIGINAL REPORT

Multicenter Phase II Study of Mogamulizumab (KW-0761), a Defucosylated Anti-CC Chemokine Receptor 4 Antibody, in Patients With Relapsed Peripheral T-Cell Lymphoma and Cutaneous T-Cell Lymphoma

Michinori Ogura, Takashi Ishida, Kiyohiko Hatake, Masafumi Taniwaki, Kiyoshi Ando, Kensei Tobinai, Katsuya Fujimoto, Kazuhito Yamamoto, Toshihiro Miyamoto, Naokuni Uike, Mitsune Tanimoto, Kunihiro Tsukasaki, Kenichi Ishizawa, Junji Suzumiya, Hiroshi Inagaki, Kazuo Tamura, Shiro Akinaga, Masao Tomonaga, and Ryuzo Ueda

Michinori Ogura, Nagoya Daini Red Cross Hospital; Takashi Ishida and Hiroshi Inagaki, Nagoya City University Graduate School of Medical Sciences; Kazuhito Yamamoto, Aichi Cancer Center; Ryuzo Ueda, Aichi Medical University School of Medicine, Nagoya; Kiyohiko Hatake, Japanese Foundation for Cancer Research; Kensei Tobinai, National Cancer Center Hospital; Shiro Akinaga, Kyowa Hakko Kirin, Tokyo; Masafumi Taniwaki, Kyoto Prefectural University of Medicine, Kyoto; Kiyoshi Ando, Tokai University School of Medicine, Kanagawa; Katsuya Fujimoto, Hokkaido University Graduate School of Medicine, Sapporo; Toshihiro Miyamoto, Kyushu University Graduate School of Medical Sciences; Naokuni Uike, National Hospital Organization Kyushu Cancer Center; Kazuo Tamura, Fukuoka University, Fukuoka; Mitsune Tanimoto, Okayama University Hospital, Okayama; Kunihiro Tsukasaki, Nagasaki University Graduate School of Biomedical Science; Masao Tomonaga, Japanese Red Cross Nagasaki Atomic Bomb Hospital, Nagasaki; Kenichi Ishizawa, Tohoku University Hospital, Sendai; and Junji Suzumiya, Shimane University Hospital, Izumo, Japan.

Published online ahead of print at www.jco.org on March 10, 2014.

Both M.O. and T.I. contributed equally to this work.

Authors' disclosures of potential conflicts of interest and author contributions are found at the end of this article.

Clinical trial information: NCT01192984.

Corresponding author: Michinori Ogura, MD, PhD, Department of Hematology and Oncology, Nagoya Daini Red Cross Hospital, 2-9 Myoken-cho, Showa-ku, Nagoya 466-8650, Japan; e-mail: mi-ogura@naa.att.ne.jp.

0732-183X/14/3211w-1157w/$20.00

DOI: 10.1200/JCO.2013.52.0924

ABSTRACT

Purpose
CC chemokine receptor 4 (CCR4) is expressed by peripheral T-cell lymphomas (PTCLs) and is associated with poor outcomes. Mogamulizumab (KW-0761) is a defucosylated humanized anti-CCR4 antibody engineered to exert potent antibody-dependent cellular cytotoxicity. This multicenter phase II study evaluated the efficacy and safety of mogamulizumab in patients with relapsed PTCL and cutaneous T-cell lymphoma (CTCL).

Patients and Methods
Mogamulizumab (1.0 mg/kg) was administered intravenously once per week for 8 weeks to patients with relapsed CCR4-positive PTCL or CTCL. The primary end point was the overall response rate, and the secondary end points included safety, progression-free survival (PFS), and overall survival (OS).

Results
A total of 38 patients were enrolled, and 37 patients received mogamulizumab. Objective responses were noted for 13 of 37 patients (35%; 95% CI, 20% to 53%), including five patients (14%) with complete response. The median PFS was 3.0 months (95% CI, 1.6 to 4.9 months), and the median OS was not calculated. The mean maximum and trough mogamulizumab concentrations (± standard deviation) after the eighth infusion were 45.9 ± 9.3 and 29.0 ± 13.3 μg/mL, respectively. The most common adverse events were hematologic events, pyrexia, and skin disorders, all of which were reversible and manageable.

Conclusion
Mogamulizumab exhibited clinically meaningful antitumor activity in patients with relapsed PTCL and CTCL, with an acceptable toxicity profile. Further investigation of mogamulizumab for treatment of T-cell lymphoma is warranted.

J Clin Oncol 32:1157-1163. © 2014 by American Society of Clinical Oncology

INTRODUCTION

Mature T/natural killer (NK)-cell neoplasms comprise approximately 20 subclassified heterogeneous groups of non-Hodgkin lymphomas (NHLs) that account for approximately 10% of NHLs in Western countries[1-3] and approximately 25% of NHLs in Japan.[4,5] Mature T/NK-cell neoplasms are largely subdivided into peripheral T-cell lymphoma (PTCL) and cutaneous T-cell lymphoma (CTCL), and different treatment strategies are used for each of these entities.[1,6]

According to the WHO classification, PTCL includes peripheral T-cell lymphoma not otherwise specified (PTCL-NOS), angioimmunoblastic T-cell lymphoma (AITL), and anaplastic large-cell lymphoma (ALCL).[1-3] Cyclophosphamide, doxorubicin, vincristine, and prednisone (CHOP) and CHOP-like regimens have been widely used as the standard first-line treatment for patients with PTCL.[7,8] With the exception of those patients with anaplastic lymphoma kinase-positive ALCL, the efficacy of these combination therapies is unsatisfactory because those who achieve remission eventually experience relapse and poor outcomes.[3,9] Several agents have been approved by the US Food and Drug Administration for the treatment of relapsed or refractory (Rel/Ref) PTCL: pralatrexate, romidepsin for Rel/Ref PTCL, and brentuximab vedotin for Rel/Ref ALCL. The overall response rates

(ORRs) were reported to be 29% and 25% for PTCL and 86% for ALCL, respectively.[10-12]

CTCL can be classified as mycosis fungoides (MF), Sézary syndrome, or cutaneous ALCL. The majority of cases of CTCL in Japan consist of MF.[13] The therapeutic approaches and outcomes for these conditions are primarily dependent on disease stage.[6,7,14] Patients with advanced stage CTCL who relapse after systemic chemotherapies and those with transformed MF have particularly poor outcomes.[15,16] Recently, the US Food and Drug Administration approved agents for Rel/Ref CTCL treatment, including vorinostat, denileukin diftitox, and romidepsin, with ORRs of 30%, 30%, and 34%, respectively.[17-19] However, there are few treatment options or approved agents for CTCL in Japan, partly because of its low prevalence here.[5,12,13]

CC chemokine receptor 4 (CCR4) is a marker for type 2 helper T cells or regulatory T (Treg) cells and is expressed on tumor cells in approximately 30% to 65% of patients with PTCL.[20,21] CCR4-positive patients (eg, in the PTCL-NOS subgroup) have a shorter survival time when compared with CCR4-negative patients.[21-23] Further, CCR4 expression increases with advancing disease stage in patients with MF/Sézary syndrome.[24]

Mogamulizumab (KW-0761) is a humanized anti-CCR4 monoclonal antibody with a defucosylated Fc region that enhances antibody-dependent cellular cytotoxicity.[25,26] In vitro antibody-dependent cellular cytotoxicity assay and in vivo studies in a humanized mouse model revealed that mogamulizumab exhibited potent antitumor activity against T-cell lymphoma cell lines and against primary CTCL cells from patients.[26-28]

In a phase I study of patients with relapsed adult T-cell leukemia-lymphoma (ATL) and PTCL/CTCL, mogamulizumab was well tolerated up to a dose of 1.0 mg/kg. An ORR of 31% (five of 16) was obtained, including one partial response (PR) among three patients with PTCL/CTCL.[29] Mogamulizumab yielded an ORR of 50% (13 of 26) for relapsed CCR4-positive ATL in a subsequent phase II study.[30] In the United States, a phase I/II study for patients with Rel/Ref CTCL revealed that mogamulizumab was well tolerated with an ORR of 37% (14 of 38, 8% complete response [CR], 29% PR) and a median PFS of 341 days.[31]

The present report describes the results of a multicenter phase II study in Japan that was designed to assess the efficacy and safety of mogamulizumab in patients with relapsed CCR4-positive PTCL or CTCL.

PATIENTS AND METHODS

Study Design and Treatment

This was a multicenter, single-arm phase II study conducted at 15 Japanese centers. At least 35 patients were required to detect a lower limit of the 95% CI that exceeded the 5% threshold, and the expected ORR for mogamulizumab was 25% with a statistical power of 90%.[10,29]

All patients gave written informed consent before enrollment. Patients received intravenous infusions of 1.0 mg/kg mogamulizumab once per week for 8 weeks. Dose modification of mogamulizumab was not allowed. Oral antihistamine and acetaminophen were given before each dose of mogamulizumab as premedication.[29,30] A systemic corticosteroid (hydrocortisone 100 mg intravenously) was also administered before the first dose of mogamulizumab to prevent an infusion reaction. The same dose of hydrocortisone was administered before the second and subsequent administrations at the investigators' discretion. The plasma concentrations of mogamulizumab and antimogamulizumab antibodies in plasma were determined by using enzyme-linked immunosorbent assays.[29,30] Blood samples were collected from all patients who received at least one dose of mogamulizumab at times determined by the protocol for pharmacokinetic analyses. Maximum plasma mogamulizumab concentration and trough concentration parameters were calculated from 0 to 7 days after the eight doses. T-cell subsets and NK cell distribution were also investigated by flow cytometry during and after mogamulizumab treatment. This study was conducted in accordance with the Declaration of Helsinki and in compliance with Good Clinical Practices. The protocol was approved by the institutional review board at each participating institution.

Patients

Patients who were ≥ 20 years of age and who had CCR4-positive PTCL or CTCL with relapse after their last systemic chemotherapy were eligible for participation. Patients who were refractory to their most recent therapy were not eligible for this study. Histopathological subtypes were assessed and reclassified by the Independent Pathology Review Committee according to the 2008 WHO classification.[1] CCR4 expression was determined by immunohistochemistry by using an anti-CCR4 monoclonal antibody (KM2160) and was confirmed by central review, as described previously.[29] In brief, CCR4 expression was classified according to the proportion of stained tumor cells (negative, < 10%; 1+, 10% to <25%; 2+, 25% to < 50%; 3+, ≥ 50%). Staging of nodal/extranodal and/or cutaneous lesions was performed if the lesions met the following requirements: nodal and extranodal lesions were > 1.5 cm in measurable length on cross-sectional computed tomography images, cutaneous lesions were identifiable on visual inspection, and peripheral blood abnormal lymphocyte count was ≥ 1,000/μL and comprised ≥ 5% of total leukocytes. All patients were required to have an Eastern Cooperative Oncology Group performance status of 0 to 2. Other notable eligibility criteria regarding laboratory values were as follows: neutrophil count ≥ 1,500/μL, platelet count ≥ 50,000/μL, hemoglobin level ≥ 8.0 g/dL, AST level ≤ 2.5× the upper limit of normal (ULN), ALT level ≤ 2.5× the ULN, total bilirubin level ≤ 1.5× the ULN, and serum creatinine level ≤ 1.5× the ULN. Patients were excluded if they had any severe complications, such as CNS involvement or a bulky lymphoma mass requiring emergent radiotherapy, a history of allogeneic stem-cell transplantation, active concurrent cancers, an active infection, or positivity for hepatitis B virus DNA, hepatitis B surface antigen, hepatitis C virus antibody, or human immunodeficiency virus antibody.

Efficacy and Safety Assessment

The primary objective was to assess the best overall response, and the secondary objectives included assessments of the best response according to disease site, progression-free survival (PFS), and overall survival (OS). Efficacy was evaluated by the Independent Efficacy Assessment Committee according to modified response criteria based on the International Working Group Criteria.[32,33] Cutaneous lesions were evaluated by using the modified Severity Weighted Assessment Tool.[34] In addition, treatment efficacy in patients with CTCL was evaluated by using a Global Response Score.[35] Responses were assessed after the fourth and eighth mogamulizumab infusions and at 2 and 4 months after the end of treatment. Treatment was discontinued if progressive disease (PD) was evident. PD and survival were monitored until at least 4 months after the completion of dosing. For safety evaluations, adverse events (AEs) were graded according to the National Cancer Institute Common Terminology Criteria for AEs, version 4.0.

Statistical Analysis

PFS and OS were analyzed by using the Kaplan-Meier method. PFS was defined as the time from the first dose of mogamulizumab to progression, relapse, or death by any cause (whichever occurred first). OS was measured from the day of the first dose to death by any cause.

RESULTS

Patient Characteristics

Sixty-five patients were screened, and 64 biopsy specimens were histologically confirmed as PTCL or CTCL by the Independent Pathology Review Committee. In total, 50 (78%) of the 64 screened

patients were CCR4-positive. Of these, 38 eligible patients were enrolled in the study and 37 received at least one infusion of mogamulizumab. One patient withdrew because of an infectious complication before dosing. Patient characteristics, histopathology subtypes, and previous systemic therapies are shown in Table 1.

Table 1. Baseline Patient Demographic and Clinical Characteristics

Characteristic*	Patients (N = 37) No.	%	Patients With PTCL (n = 29) No.	%	Patients With CTCL (n = 8) No.	%
Age, years						
Median	64		67		50	
Range	33-80		33-80		36-70	
≥ 65	18	49	17	59	1	13
Sex						
Male	23	62	20	69	3	38
Female	14	38	9	31	5	63
ECOG performance status						
0	24	65	19	66	5	63
1	12	32	10	34	2	25
2	1	3	0	0	1	13
Elevated LDH level†	21	57	18	62	3	38
Bone marrow involvement	7	19	7	24	0	0
No. of previous systemic regimens						
Median	2		2		3	
Range	1-6		1-5		1-6	
1	14	38	13	45	1	13
2	15	41	12	41	3	38
≥ 3	8	22	4	14	4	50
Types of systemic therapy						
Chemotherapy	37	100	29	100	8	100
CHOP/CHOP-like regimen	36	97	29	100	7	88
DeVIC	6	16	4	14	2	25
CHASE	5	14	5	17	0	0
Single-agent therapy	5	14	0	0	5	63
Other	10	27	10	34	0	0
Auto-PBSCT	3	8	3	10	0	0
Radiotherapy	9	24	5	17	4	50
Intensity of CCR4 expression‡						
1+	6	16	4	14	2	25
2+	6	16	4	14	2	25
3+	25	68	21	72	4	50
Histopathology by central review						
PTCL-NOS	16	43	16	55		
AITL	12	32	12	41		
ALCL, ALK negative	1	3	1	4		
MF	7	19			7	88
c-ALCL	1	3			1	13

Abbreviations: AITL, angioimmunoblastic T-cell lymphoma; ALCL, anaplastic large-cell lymphoma; ALK, anaplastic lymphoma kinase; c-ALCL, cutaneous anaplastic large-cell lymphoma; CHASE, cyclophosphamide, cytosine arabinoside, etoposide, and dexamethasone; CHOP, cyclophosphamide, doxorubicin, vincristine, and prednisone; CTCL, cutaneous T-cell lymphoma; DeVIC, dexamethasone, etoposide, ifosfamide, and carboplatin; ECOG, Eastern Cooperative Oncology Group; LDH, lactate dehydrogenase; MF, mycosis fungoides; NOS, not otherwise specified; PBSCT, peripheral-blood stem-cell transplantation; PTCL, peripheral T-cell lymphoma.

*Of the 38 patients enrolled, 37 received at least one infusion of mogamulizumab.

†Elevated LDH level: higher LDH level than upper limit of the normal range.

‡The denominator used for the intensity of CC chemokine receptor 4 (CCR4) expression is based on subjects who were positive for CCR4 by immunohistochemistry.

Of the 37 patients who received mogamulizumab, 25 (68%) completed the planned course of eight infusions. Nine patients (24%) discontinued treatment because of PD, and three patients (8%) due to serious AEs.

Efficacy

The ORR for the 37 treated patients was 35% (13 of 37; 95% CI, 20% to 53%), and 14% of patients (five of 37) achieved a CR, of which one was unconfirmed (Table 2). Reponses (CR/PR) were observed in at least one patient with each subtype of disease, but the ORR differed between subtypes. The ORR was 34% (10 of 29; 95% CI, 18% to 54%) in patients with PTCL (three of 16 for PTCL-NOS, six of 12 for AITL, and one of one for ALCL, anaplastic lymphoma kinase-negative) and 38% (three of eight; 95% CI, 9% to 76%) in those with CTCL (two of seven for MF and one of one for cutaneous ALCL). In addition, ORR in patients with CTCL was 50% (four of eight; 95% CI, 16% to 84%) according to the Global Response Score.

Total ORR did not significantly correlate with CCR4 expression level, patient age, or the number of previous chemotherapy regimens. The response rates for lymph node and cutaneous lesions were 33% (11 of 33) and 58% (seven of 12), respectively.

The median PFS was 3.0 months (95% CI, 1.6 to 4.9 months) for the entire population and 2.0 months for patients with PTCL. Although the median OS was not reached for the entire population at the

Table 2. Best Response (N = 37)

Parameter	No. of Patients	No. of Patients With Best Response CR/CRu	PR	SD	PD	Response Rate (%)*
Overall response	37	5	8	13	11	35
Histopathology by central review						
PTCL	29	5†	5	9	10	34
PTCL-NOS	16	1	2	6	7	19
AITL	12	3	3	3	3	50
ALCL, ALK negative	1	1†	0	0	0	100
CTCL	8	0	3	4	1	38
MF	7	0	2	4	1	29
c-ALCL	1	0	1	0	0	100
Age, years						
< 65	19	1†	6	7	5	37
≥ 65	18	4	2	6	6	33
Intensity of CCR4 expression						
1+	6	1	1	3	1	33
2+	6	1	2	2	1	50
3+	25	3†	5	8	9	32
No. of previous systemic regimens						
1	14	3	3	6	2	43
2	15	1	1	6	7	13
≥ 3	8	1†	4	1	2	63

Abbreviations: AITL, angioimmunoblastic T-cell lymphoma; ALCL, anaplastic large-cell lymphoma; ALK, anaplastic lymphoma kinase; c-ALCL, cutaneous anaplastic large-cell lymphoma; CCR4, CC chemokine receptor 4; CR, complete response/complete remission; CRu, uncertain complete response/uncertain complete remission; CTCL, cutaneous T-cell lymphoma; MF, mycosis fungoides; NOS, not otherwise specified; PD, progressive disease; PR, partial response/partial remission; PTCL, peripheral T-cell lymphoma; SD, stable disease.

*Response rate (%): 100 × number of responders/number of subjects in each category included in the efficacy analysis set.

†Among the patients who showed CR/CRu, one showed CRu.

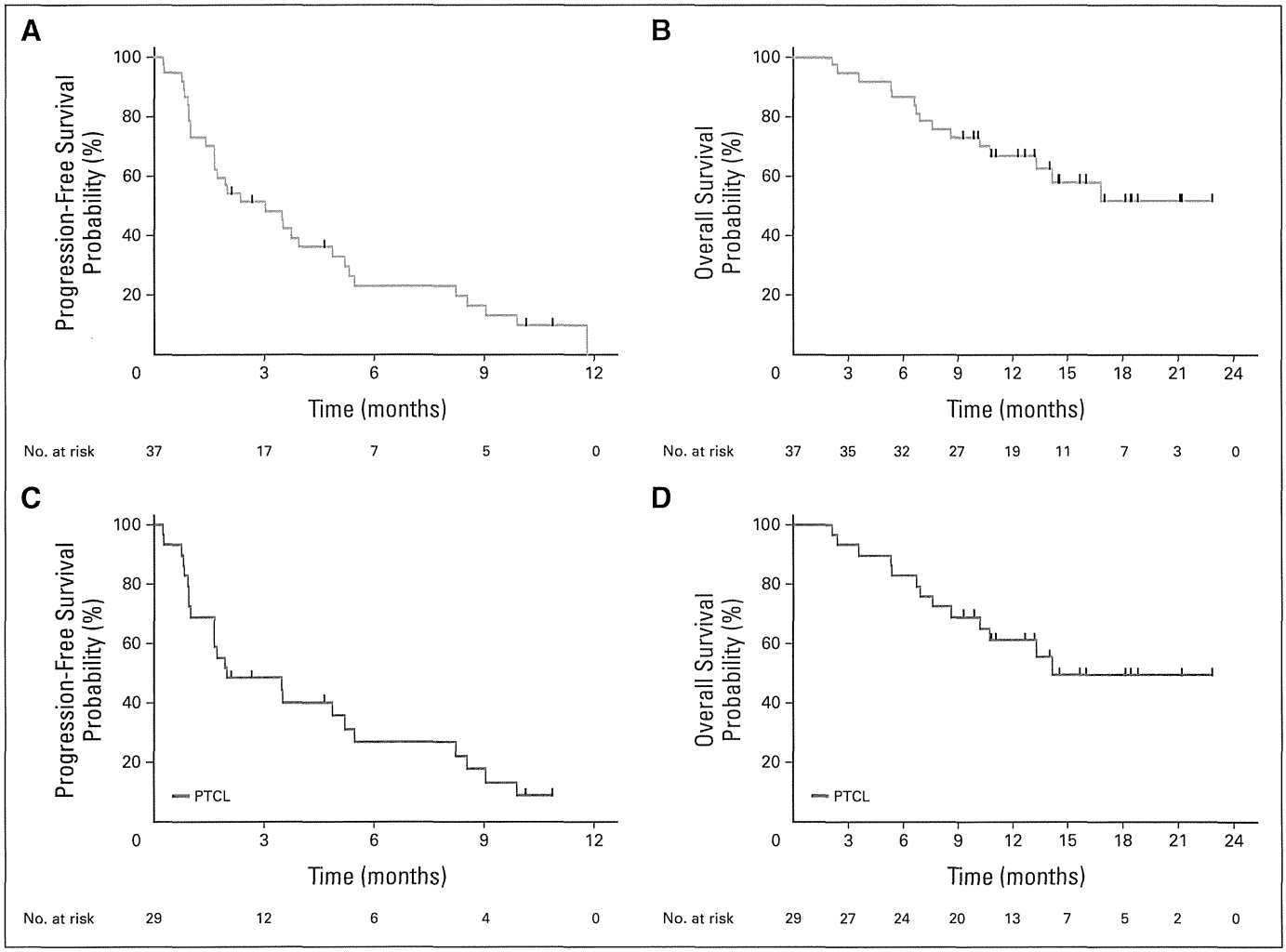

Fig 1. Kaplan-Meier curves of (A) estimated progression-free survival (median, 3.0 months), (B) overall survival (median not reached), (C) progression-free survival in patients with peripheral T-cell lymphoma (PTCL; median, 2.0 months), and (D) overall survival in patients with PTCL (median, 14.2 months).

time of this report, it was 14.2 months for patients with PTCL (Fig 1). Moreover, the median PFS of all 13 responders was 5.5 months, and for PTCL responders (n = 10), it was 8.2 months.

Safety

The most common treatment-related AEs of all grades and treatment-related AEs of grade 3/4 were lymphocytopenia (81%, 73%), neutropenia (38%, 19%), and leukocytopenia (43%, 14%), whereas the most common nonhematologic AE was pyrexia (30%; grade 2 or lower) (Table 3). Lymphocytopenia occurred in 30 patients (81%) and was noted after the first dose in 26 of these patients. For 19 of the patients, lymphocyte counts were $< 800/\mu L$ (grades 2 to 4) before the first dosing. The lymphocyte count ultimately recovered to normal or baseline levels in all patients.

Infusion reaction (24%; grade 2 or lower) occurred primarily at the first infusion, after which it became less frequent, and all patients recovered. No infusion prolongation/interruption was caused by the infusion reaction.

In addition, treatment-related skin disorders were commonly reported (all grades, 51%; grade 3/4, 11%) when grouped according to system organ class. Of the 19 patients who suffered from skin disorder complications, 15 patients experienced improvement, whereas the remaining patients discontinued treatment because of PD or switched to other post treatments. One patient who had a history of psoriasis before the study treatment developed two serious skin disorders (toxicoderma and psoriasis vulgaris) during the study period.

Fifteen serious treatment-related AEs were observed among eight patients (22%); these AEs included grade 3 polymyositis in one patient, grade 2 cytomegalovirus retinitis in two patients, and grade 4 second primary malignancy in one patient with AITL. All patients improved over time, and there were no deaths related to AEs.

Pharmacokinetics and Pharmacodynamics

The mean maximum mogamulizumab concentration and trough mogamulizumab concentration (± standard deviation) in plasma after the eighth infusion were 45.9 ± 9.3 and 29.0 ± 13.3 $\mu g/mL$, respectively. Antimogamulizumab antibodies were not detected after dosing in any patients. These results were consistent with the findings of a previous study of patients with ATL.[30] As an exploratory study, we assessed the effect of mogamulizumab on the number of CD4+/CD25+/Foxp3+ cells (the Treg cell subset) and CD45+/CD16+/CD56+ cells (the NK cell subset). Patients given

